URSI UK Symposium 2024

National Physical Laboratory

Hampton Road

Teddington, Middlesex TW11 0LW

10:00 am – 5:30 pm on 21 February 2024

Symposium Programme and Proceeding

Chair: Prof Tian Hong Loh

Co-Chair: Prof Yang Hao

Symposium Programme

09:30 – 10:00	Registrations and Coffee	
10:00 – 12:00 Session 1: Oral Presentations Chair: Professor Yang Hao (Queen Mary University of London, UK)		
10:00 – 10:10	Tian Hong Loh (National Physical Laboratory, UK)	Opening Remarks, Introduction to URSI, Welcome and Site Information
10:10 – 10:40	Yuanwei Liu (Queen Mary University of London, UK)	**Keynote Speech:** Simultaneously Transmitting and Reflecting Surface (STARS) for 360° Coverage
10:40 – 11:00	Chika Worka (University of Huddersfield, UK)	Reconfigurable Intelligent Surfaces (RISs) Assisted Non-Terrestrial Networks (NTNs) based 6G Communications
11:00 – 11:20	Tony Knightley, Alex Yakovlev, and Victor Pacheco-Peña (Newcastle University, UK)	Temporal differential operator emulated by neural network designed multiplayer metamaterial
11:20 – 11:40	Valentina Cicchetti (Queen Mary University of London, UK)	3D Printed Wideband Dual-Polarized Lens Antenna for mm-Wave Communication
11:40 – 12:00	Lawrence Carslake, James Skinner, and Tian Hong Loh (National Physical Laboratory, UK)	Design and Preliminary Indoor Assessment of a Long-Range sub-THz VNA-Based Channel Sounder between 500 GHz and 750 GHz
12:00 – 12:40 Session 2: Lunch and Poster Presentations Chair: Dr Yuanwei Liu (Queen Mary University of London, UK)		
Poster P1-1	Jiahao.Hu (Durham University, UK), Silvi Kodra (University of Bologna, Italy) and Sana Salous (Durham University, UK)	Multi-frequency Measurements of Material Reflection and Penetration Losses
Poster P1-2		

	Joseph A. Riley (Newcastle University, UK), M. Horák (Brno University of Technology, Czech Republic), R. G. Macdonald (Newcastle University, UK), C. Johnson-Richards (Newcastle University, UK), N. Healy (Newcastle University, UK), V. Křápek (Brno University of Technology, Czech Republic), and V. Pacheco-Peña (Newcastle University, UK)	On the performance of plasmonic sensors enabled by Babinet's principle
Poster P1-3	Dou Feng, Christopher Sumner, Morgan Dryhurst, Jie Qing, Olcay Altıntaş, Aleksandr Bystrov, and Miguel Navarro Cía (University of Birmingham, UK)	Building a reliable THz material library
Poster P1-4	Ibrahim Gharbia, Atta Ullah, Abubakar Salisu, and Raed A. Abd-Alhameed (University of Bradford, UK)	Multi-band UHF RFID Reader Antenna Design
Poster P1-5	Abubakar Salisu (University of Bradford, UK & MAU Yola, Nigeria), Atta Ullah (University of Bradford, UK), Umar Musa (Bayero University Kano, Nigeria), Mobayode O. Akinsolu (Wrexham Glyndwr University, UK), Ibrahim Gharbia (University of Bradford, UK), Ahmad Aldelemy (University of Bradford, UK), A. S. Hussaini (University of Bradford, UK & American University of Nigeria, Nigeria), and Raed A. Abd-Alhameed (University of Bradford, UK).	Reconfigurable Dual Band Antenna with Ultra-wide Bandwidth Operating at Sub 6GHz and Millimeter Wave Bands For 5G Mobile Applications
Poster P1-6	Murray Brown and Hongjian Sun (Durham University, UK)	Compact Implantable Antenna Design for Leadless Cardiac Pacemaker System
Poster P1-7	Abdullah Alshammari, Amjad Iqbal, Roy B.V.B. Simorangkir, and Ismail Ben Mabrouk (Durham University, UK)	Ultra-Miniaturized In-Band Full-Duplex Implantable Antenna for Wireless Capsule Endoscopy
Poster P1-8	Eryk S. Skalinski, Roy B. V. B. Simorangkir, and Ismail Ben Mabrouk (Durham University, UK)	300 GHz Stacked AFSIW LTCC Horn Array Antenna with Integrated Lenses for V2V
Poster P1-9	Abdulwahab Alghamdi, Roy B. V. B. Simorangkir, and Ismail Ben Mabrouk (Durham University, UK)	Compact Implantable Antenna with Ultra-wide bandwidth for Leadless Pacemaker

Poster P1-10	Sihao Chen, Liyang Yu, and Wen Dang (Hangzhou DianZi University, China)	Ultrashort Electromagnetic Pulse System for Biological Application
Poster P1-11	Zhaolin Wang, Xidong Mu, Yuanwei Liu (Queen Mary University of London, UK)	Near-Field Velocity Sensing
Poster P1-12	Liu Chang (Durham University, UK), Amjad Iqbal (Durham University, UK), Abdul Basir (Tampere University, Finland), Roy B. V. B. Simorangkir (Durham University, UK), and Ismail Ben Mabrouk (Durham University, UK)	A Compact Conformal Capsule Antenna For MIMO Operation
Poster P1-13	Haleh J. Basherlou, N. O. Parchin, L. Manjakkal, C. H. See (Edinburgh Napier University, UK), and R. A. Abd-Alhameed (University of Bradford)	Multiple-Element Smartphone Antenna Design with Broadband Resonators for 5G Cellular Communications in Sub 6 GHz Spectra
Poster P1-14	Martins Odiamenhi, C.H. See, N. Ojaroudi Parchin, H. Yu, and K. Goh (Edinburgh Napier University, UK)	A Multiple-stage Uniform Transmission Line Matching Technique for Triple-Band RF-to-DC Rectifier with Harmonic Suppression for Wireless Power Transfer Applications
Poster P1-15	Muhammad Qamar (Queen Mary University of London, UK), Kamil Yavuz Kapusuz (Ghent University, Belgium), Mohamed A. Thaha (Queen Mary University of London, UK), and Akram Alomainy (Queen Mary University of London, UK)	Challenges in Camera Integrated Antenna Design for WCE
Poster P1-16	Qi Li (Beijing University of Posts and Telecommunications, China & National Physical Laboratory, UK), Ben Chen (Beijing Jiaotong University, China), Ke Guan (Beijing Jiaotong University, China), Lawrence Carslake (National Physical Laboratory, UK), Yuan Yao (Beijing University of Posts and Telecommunications, China), and Tian Hong Loh (National Physical Laboratory, UK)	A Ray Tracing Channel Modelling Study for Indoor Sub-THz Propagation between 500 GHz and 750 GHz
Poster P1-17	William J. Bourne, Roy B. V. B. Simorangkir, and Ismail Ben Mabrouk (Durham University, UK)	Optimising Optical Transparancy and RF Performance in Meshed 5G Vehicular Antennas

12:40 – 14:20 Session 3: Oral Presentations Chair: Prof Anna Scaife (University of Manchester, UK)		
12:40 – 13:00	Roland Timmerman (Durham University, UK)	Radio-mode feedback in high-redshift galaxy clusters with the International LOFAR Telescope
13:00 – 13:20	James Petley and Leah Morabito (Durham University, UK)	Understanding Supermassive Black Hole Outflows with International LOFAR
13:20 – 13:40	Sophie J. Maguire, A. G. Wood, D. R. Themens (University of Birmingham, UK), and D. McKay (Aalto University, Finland)	Observing plasma structures at multiple scale sizes in the high-latitude ionosphere with a suite of ground-based instrumentation
13:40 – 14:00	William McGenn (University of Manchester, UK), Hui Wang (Rutherford Appleton Laboratory, UK), Elle Franks (University of Manchester, UK), Brian Ellison (University of Manchester, UK), Gary A. Fuller (University of Manchester, UK), Danielle George (University of Manchester, UK), Peter G. Huggard (Rutherford Appleton Laboratory, UK)	Low Noise Amplifier Based Heterodyne Highly Integrated Receivers for Millimetre and Sub-millimetre Wavelength Radio Astronomy
14:00 – 14:20	Emmy Escott (Durham University, UK)	Unveiling AGN Outflows: [O III] Detection Rates and their Correlation with Low-Frequency Radio Emission
14:20 – 15:00 Session 4: Coffee and Poster Presentations Chair: Dr Keyur Mistry (Mangata Networks, UK)		
Poster P2-1	Alex Ventisei, Alex Yakovlev, and Victor Pacheco-Peña (Newcastle University, UK)	Design and Modelling of Waveguide Junction Topologies with Petri-Nets for Computing Applications
Poster P2-2	William Rogers, Christian Johnson-Richards, Alex Yakovlev, and Victor Pacheco-Peña (Newcastle University, UK)	Interconnected rectangular waveguides and their potential for perfect splitters
Poster P2-3	Rachel Black (University of Exeter, UK & British Antarctic Survey, UK), Oliver Allanson (University of Birmingham, UK & University of	Investigating the variability of chorus waves in the radiation belts for improved understanding of nonlinear interactions

	Exeter, UK), Nigel Meredith (British Antarctic Survey, UK), and Andrew Hillier (University of Exeter, UK)	
Poster P2-4	Ross Glyn MacDonald, Alex Yakovlev, and Victor Pacheco-Peña (Newcastle University, UK)	Towards partial differential equation solvers using light-matter interactions
Poster P2-5	Christian Johnson-Richards, Alex Yakovlev, and Victor Pacheco-Peña (Newcastle University, UK)	Scattering Matrix Evaluation of a 6-port Valley Photonic Crystal
Poster P2-6	Ben Boyde, Alan G. Wood, Gareth Dorrian (University of Birmingham), Francesco de Gasperin (INAF - Istituto di Radioastronomia, Italy & University of Hamburg, Germany), Frits Sweijen (Leiden University, The Netherlands), Maaijke Mevius, and Kasia Beser (ASTRON – The Netherlands Institute for Radio Astronomy, The Netherlands)	Statistics of Small-Scale Ionospheric Waves in European Mid-Latitudes Observed Using LOFAR
Poster P2-7	Prince O. Siaw (University of Bradford, UK), Mohamed Lashab (University of Oum El Bouagui, Algeria), Ebenezer Adjei (University of Bradford, UK), Ahmad Aldelemy (University of Bradford, UK), Raed A. Abd-Alhameed (University of Bradford, UK)	Optimized Design of a Compact Rectangular Metamaterial Sensor for Bone Fracture Detection
Poster P2-8	Ali Ghaffarlouy Raef, Andy Marvin, Martin Robinson, Simon Bale, and John Dawson (University of York, UK)	Shielding Effectiveness of Reverberant Equipment Enclosures Measured in Reverberation Chamber
Poster P2-9	Natalie Reeves (University of Birmingham, UK)	Understanding the sensitivity of the thermosphere and ionosphere to solar and geomagnetic conditions using Global Sensitivity Analysis Techniques
Poster P2-10	Zohreh Ebadi (Queen's University of Belfast, UK)	Near-Field Localization with an Exact Propagation Model in the Presence of Mutual Coupling
Poster P2-11	Rahul Dutta, Flynn Castles, and Yang Hao (Queen Mary University of London, UK)	Towards Minimal Negative Static Electric Susceptibility: Crystal Engineering in Active Metamaterials
Poster P2-12	Sanchita Kayal, Geoffrey Hilton, and Mark Beach (University of Bristol, UK)	A RF Propagation Modelling Methodology for Determining the Level and Nature of Scattering from Measurements

Poster P2-13	Elle Franks, W. McGenn, C. Jarufe, L. Jiang, G.A. Fuller, D. George (University of Manchester, UK)	Low Noise Amplifier Characterisation Automation with the CryoMe Software Package
Poster P2-14	Samuel Boardman (University of Birmingham, UK), Oliver Allanson (University of Birmingham, UK), Adnane Osmane (University of Helsinki, Finland) and Sean Elvidge (University of Birmingham, UK)	Extending Quasilinear Theory for Particles Near 90°
Poster P2-15	Ebenezer Adjei, Prince O. Siaw, Ahmad Aldelemy, Raed A. Abd-Alhameed (University of Bradford) and, Mohamed Lashab (University of Oum El Bouagui, Algeria)	Enhancing Patient Monitoring Systems Through Differential Power Gains and Time Delay Series emanating from RFID Sensors
Poster P2-16	Francesco Lisi (Heriot-Watt University, UK), Carol Marsh (Celestia UK, UK), Ed Totten (Celestia UK, UK), and George Goussetis (Heriot-Watt University, UK)	Linear Precoding as an Interference Mitigation Technique in a Phased Array Gateway for large LEO Constellations
15:00 – 16:40 Session 5: Oral Presentations Chair: Dr Chan Hwang See (Edinburgh Napier University, UK)		
15:00 – 15:20	Elif Dogu (Queen Mary University of London, UK), Jose A. Paredes (University of Roehampton, UK), Akram Alomainy (Queen Mary University of London, UK), Janelle M. Jones (Queen Mary University of London, UK) and Khalid Z. Rajab (Queen Mary University of London, UK)	Falls Risk Screening with Millimetre-Wave Radar
15:20 – 15:40	Ahmad Aldelemy, Prince O. Siaw, Ebenezer Adjei, Raed A. Abd-Alhameed (University of Bradford)	Real-time Monitoring of Femur Fractures with AI-enhanced RF Sensors
15:40 – 16:00	Oscar Sage David O'Hara, Fred Dulwich, Jiten Dhandha, Thomas Gessey-Jones, Anastasia Fialkov, Eloy de Lera Acedo (University of Cambridge, UK)	Understanding spectral artefacts in SKA-LOW 21-cm cosmology experiments: the impact of cable reflections
16:00 – 16:20	Isabella Langdon and Martin Robinson (University of York, UK)	Non-destructive identification of archeological objects using resonant cavity perturbation technique

16:20 – 16:40	Joseph Arnold Riley, Christian Johnson-Richards, Noel Healy, and Victor Pacheco-Peña (Newcastle University, UK)	Electromagnetic properties of additive manufactured polymers at telecommunication wavelengths
16:40 – 17:20	Tour of NPL Laboratories	
17:20 – 17:30	Award of Prizes and Closing Remarks	

URSI UK Symposium 2024 Proceeding

URSI UK Symposium 2024, 21 February 2024

Multi-frequency Measurements of Material Reflection and Penetration Losses

Jiahao.Hu[(1)], Silvi Kodra[(2)] and Sana Salous[(1)]
(1) Department of Engineering, Durham University, Durham, United Kingdom sanasalous@durham.ac.uk
(2) Department of Electrical, Electronic, and Information Engineering "Guglielmo Marconi"(DEI),CNIT, University of Bologna, Italy

Considering the present and future 5G and 6G multi-band communications, achieving seamless indoor wireless coverage is an important challenge in particular between different floors and partitions. Various measurement setups have been reported in the literature to estimate the penetration and reflection losses [1]-[3]: in [1] for 28, 39, 120 and 140 GHz, in [2] for 60, 73 and 81 GHz, and in [3] for 28 and 39 GHz. Within this context, continuous wave measurements were conducted to estimate the penetration and reflection loss of six different materials in indoor scenarios at 25, 77 and 153 GHz.

The measurements were performed using the custom designed setup at Durham University to generate a Continuous wave (CW) signal at 25.6 GHz ,77 GHz and 153 GHz, respectively. For setting up the penetration loss measurements, the transmitter and receiver were facing each other at a distance of 3.6 meters, while the materials were held on an aligned frame in the middle of their direct path. The reflection loss measurements were conducted where the transmitter and the receiver were placed at 45 degrees towards the center of the material. To perform the reflection loss measurements, an aluminum sheet of the same specifications with other materials was taken as a reference (considered a total reflector). Table 1 shows penetration and the reflection loss of different materials, which indicates that the reflection loss is much higher than the penetration loss and both reflection and penetration loss increase with frequency, except in the case of wood floor and single glass.

Table 1. Penetration Loss and Reflection Loss (in Red) of Different Materials in (dB)

Frequency	12 mm MDF	14 mm Wood Flooring	13mm Gypsum Plasterboard	4 mm Plexiglass	3mm Plywood	4mm Single Glass	24mm Double Glazed Glass
28 GHz	1.98, (6.04)	4.02, (9.52)	1.06 (7.66)	0.12 (11.23)	1.35 (7.97)	1.49 (2.33)	13.27 (0.513)
77 GHz	5.43, (8.54)	7.23, (7.85)	1.28 (9.37)	0.71 (8.03)	2.73 (8.66)	4.06 (13.06)	18.65 (2.29)
153 GHz	7.25, (10.35)	11.26 (10.29)	1.41 (11.06)	1.14 (10.2)	4.64 (8.33)	5.96 (6.91)	23.06 (5.037)

1. Khatun, et,al ,“Indoor and outdoor penetration loss measurements at 73 and 81 ghz,” in 2019 IEEE Global Communications Conference (GLOBECOM), 2019, pp. 1–5.

2. G. Barb, F. Danuti, M. A. Ouamri, and M. Otesteanu,“Analysis of vegetation and penetration losses in 5g mmwave communication systems,” in 2022 Interna-tional Symposium on Electronics and Telecommunications (ISETC), 2022, pp. 1–5.

3. S. El Faitori and S. Salous, "Reflection and Penetration Loss Wideband Measurements of Building Materials at 28 GHz and 39 GHz," 2022 16th EuCAP, Madrid, Spain, 2022, pp. 1-4.

Unveiling AGN Outflows: [O III] Detection Rates and their Correlation with Low-Frequency Radio Emission

Emmy Escott, Durham University

The nature of radio emission from radio quiet AGN (Active Galactic Nuclei) and how AGN feedback operates are two of the unsolved mysteries plaguing modern day radio astronomy. AGN show signatures of outflows which could explain how this feedback operates. The [OIII] emission line is a common tracer of ionised outflows and studies have connected [OIII] emission to the presence of radio emission. With radio surveys deeper than ever before, we can ask: What physical process causes the connection between [OIII] and radio emission?

An instrument which can guide us closer to the answer is the ILT (International LOFAR Telescope). Using radio detected AGN in the LoTSS (LOFAR Two-meter Sky Survey) Deep Fields, I compare the outflow properties and kinematics of 75 radio detected AGN at $z < 0.83$ to 47 radio non-detected AGN. We discover that 75% of radio detected AGN host an outflow compared to 56% of radio non-detected AGN, indicating that radio detected AGN are more likely to host an [OIII] outflow compared to radio non-detected AGN.

To understand the origin of radio emission from radio quiet AGN, we use VLBI (Very Long Baseline Interferometry) techniques. I will present the first high resolution image at 144 MHz of the Boötes Deep Field.

Design and Modelling of Waveguide Junction Topologies with Petri-Nets for Computing Applications

Alex Ventisei[1, 2], Alex Yakovlev[2], and Victor Pacheco-Peña[1],

1. *School of Mathematics, Statistics and Physics, Newcastle University, Newcastle Upon Tyne, NE1 7RU, United Kingdom;*
2. *School of Engineering, Newcastle University, Newcastle Upon Tyne, NE17RU, United Kingdom*

There is a growing interest in wave-based computing as an alternative to classical computing [1]. The application of waveguide junctions with transverse electromagnetic pulses (TEM) has been shown to perform pulse routing and switching operations, fundamental to emulating classical computing systems [2], [3]. Current research on combinations of waveguide junctions in cascaded configurations for the purpose of EM computing relies heavily on full-wave simulation methods. As the topologies of waveguide junctions become larger to emulate more complex computing processes, application of full-wave simulations may require more time and energy to compute. In this work, we exploit Petri-Nets (PNs) to aid the design and potential simulation of waveguide junction topologies. PNs are a graphical modelling system [4] which has been used to represent dynamic systems in a broad range of research areas such as chemistry [5] and verification of asynchronous computing circuits [6]. Because PNs are mathematically considered as matrices, they can be used to directly map scattering matrices of waveguide junctions to PN layouts [7]. Here, we explore how PNs can be utilised to represent and analytically model individual waveguide junctions. It will also be shown how this PN representation can be extended to represent interconnected waveguide junctions with potential applications in wave-based computing. More details of PNs and how this mapping is performed will be given in the conference.

References

[1] H. J. M. Veendrick, *Nanometer CMOS ICs: From Basics to ASICs*. Heeze, The Netherlands: Springer Nature, 2017. doi: 10.1007/978-3-319-47597-4.

[2] R. G. MacDonald, A. Yakovlev, and V. Pacheco-Peña, “Amplitude-Controlled Electromagnetic Pulse Switching Using Waveguide Junctions for High-Speed Computing Processes,” *Advanced Intelligent Systems*, vol. 4, no. 12, p. 2200137, Dec. 2022, doi: 10.1002/aisy.202200137.

[3] A. Yakovlev and V. Pacheco-Peña, “Enabling High-Speed Computing with Electromagnetic Pulse Switching,” *Adv Mater Technol*, vol. 5, no. 12, p. 2000796, Dec. 2020, doi: 10.1002/admt.202000796.

[4] W. Reisig, “Understanding Petri nets,” *IEEE Parallel and Distributed Technology*, vol. 3, no. 3, pp. 54–55, 1995, doi: 10.1109/M-PDT.1995.414862.

[5] D. Angeli, P. De Leenheer, and E. D. Sontag, “A Petri net approach to the study of persistence in chemical reaction networks,” *Math Biosci*, vol. 210, no. 2, pp. 598–618, 2007, doi: 10.1016/j.mbs.2007.07.003.

[6] I. Poliakov, A. Mokhov, A. Rafiev, D. Sokolov, and A. Yakovlev, “Automated verification of asynchronous circuits using circuit Petri nets,” *Proceedings - International Symposium on Asynchronous Circuits and Systems*, no. April, pp. 161–170, 2008, doi: 10.1109/ASYNC.2008.18.

[7] A. Ventisei, A. Yakovlev, and V. Pacheco-Peña, “Exploiting Petri Nets for Graphical Modelling of Electromagnetic Pulse Switching Operations,” *Adv Theory Simul*, vol. 5, no. 3, p. 2100429, Mar. 2022, doi: 10.1002/adts.202100429.

Interconnected rectangular waveguides and their potential for perfect splitters

William Rogers [1], **Christian Johnson-Richards** [1] **Alex Yakovlev** [2], **Victor Pacheco-Peña** [1]
1 School of Mathematics, Statistics and Physics, Newcastle University, NE1 7RU, Newcastle Upon Tyne, United Kingdom;
2 School of Engineering, Newcastle University, NE1 7RU, Newcastle Upon Tyne, United Kingdom

Recent examples in the field of photonic computing include devices for solving quadratic optimization problems [1], differentiation and integration [2], [3], and optical neural networks [4]. The perfect splitting of electromagnetic (EM) waves at a junction of waveguides has also been shown to enable the design of photonic computing devices. For example, to solve partial differential equations [5] and to perform information routing and comparison operations [6], [7]. The structures in these works have been implemented using parallel plate waveguides which allow the perfect splitting of EM signals as they exhibit a large wavelength to waveguide width ratio. In this work, we propose and explore a structure that enables perfect splitting with interconnected rectangular waveguides.

The cut-off frequency of rectangular waveguides poses a challenge to achieve perfect splitting. This is due to it is defined as $\lambda_c = 2a$, where a is the width of the waveguide, limiting the wavelength to waveguide width ratio to 2:1 [8]. The result is, in a four-port example, that the majority of transmission is obtained to the port opposite the input port, i.e., imperfect splitting. To overcome this challenge, we propose a method of perfect splitting whereby a rectangular waveguide junction, operating below the cutoff frequency of the connected waveguides, is excited by evanescent coupling from an outer waveguide operating above its cut-off frequency [9]. It will be shown how this method can be applied to rectangular waveguide junctions with *N* ports, and the use of this structure for routing and comparison operations.

References

[1] K. P. Kalinin *et al.*, "Analog Iterative Machine (AIM): using light to solve quadratic optimization problems with mixed variables," *arXiv:2304.12594*, Apr. 2023.
[2] N. M. Estakhri, B. Edwards, and N. Engheta, "Inverse-designed metastructures that solve equations," *Science (1979)*, vol. 363, no. 6433, pp. 1333–1338, 2019, doi: 10.1126/science.aaw2498.
[3] A. Pors, M. G. Nielsen, and S. I. Bozhevolnyi, "Analog computing using reflective plasmonic metasurfaces," *Nano Lett*, vol. 15, no. 1, pp. 791–797, Jan. 2015, doi: 10.1021/NL5047297/ASSET/IMAGES/LARGE/NL-2014-047297_0007.JPEG.
[4] Y. Zuo *et al.*, "All-optical neural network with nonlinear activation functions," *Optica*, vol. 6, pp. 1132–1137, 2019, doi: 10.1364/OPTICA.6.001132.
[5] E. Feigenbaum and H. A. Atwater, "Resonant guided wave networks," *Phys Rev Lett*, vol. 104, no. 14, p. 147402, 2010, doi: 10.1103/PhysRevLett.104.147402.
[6] A. Yakovlev and V. Pacheco-Peña, "Enabling High-Speed Computing with Electromagnetic Pulse Switching," *Adv Mater Technol*, vol. 5, no. 12, Dec. 2020, doi: 10.1002/ADMT.202000796.
[7] R. G. MacDonald, A. Yakovlev, and V. Pacheco-Peña, "Amplitude-Controlled Electromagnetic Pulse Switching Using Waveguide Junctions for High-Speed Computing Processes," *Advanced Intelligent Systems*, vol. 4, no. 12, p. 2200137, Dec. 2022, doi: 10.1002/AISY.202200137.
[8] D. Pozar, *Microwave Engineering*, 4th ed. John Wiley & Sons, Inc., 2011.
[9] W. Rogers, C. Johnson-Richards, A. Yakovlev, and V. Pacheco-Peña, "Perfect Splitting in Rectangular Waveguide Junctions for Analogue Computing," Oct. 2023, *arXiv:2310.09317*.

Temporal differential operator emulated by neural network designed multiplayer metamaterial

Tony Knightley[1], Alex Yakovlev[2], and Victor Pacheco-Peña[1]

1. *School of Mathematics, Statistics and Physics, Newcastle University, Newcastle Upon Tyne, NE1 7RU, United Kingdom;*
2. *School of Engineering, Newcastle University, Newcastle Upon Tyne, NE1 7RU, United Kingdom;*

In recent years, metamaterials (MTMs) have gained significant interest as a means of manipulating wave-matte interactions [1]. Applications in this field include invisibility cloaking [2], lenses [3], [4], [5] and antennas [6], to name a few. Research and innovation in the field of MTMs has also enabled the proposal and demonstration of wave-based computing, with recent works reporting logic-based waveguide networks [7], [8] as well as analog signal processors for performing mathematical operations such as differentiation [9], [10], integration [11] and equation solving [12], [13].

In this communication, we use deep learning techniques to design a multilayer MTM with the capability to perform temporal differentiation on an incident electromagnetic signal [10]. By training a neural network to accurately predict the transfer function of arbitrary candidate designs, we obtain a multilayer structure that emulates the transfer function of a temporal in the frequency domain, achieving a mean squared error of $\sim 4 \times 10^{-4}$.

References

[1] N. Engheta and R. W. Ziolkowski, *Metamaterials: Physics and Engineering Explorations*. Wiley-IEEE Press, 2006. doi: 10.1007/978-3-319-48933-9_56.

[2] R. Fleury and A. Alù, "Cloaking and invisibility: A review," *Progress in Electromagnetics Research*, vol. 147, pp. 171–202, 2014, doi: 10.2528/PIER15011403.

[3] V. Pacheco-Peña, N. Engheta, S. Kuznetsov, A. Gentselev, and M. Beruete, "Experimental Realization of an Epsilon-Near-Zero Graded-Index Metalens at Terahertz Frequencies," *Phys Rev Appl*, vol. 8, no. 3, p. 034036, Sep. 2017, doi: 10.1103/PhysRevApplied.8.034036.

[4] V. Torres *et al.*, "Terahertz epsilon-near-zero graded-index lens," *Opt Express*, vol. 21, no. 7, p. 9156, Apr. 2013, doi: 10.1364/OE.21.009156.

[5] J. B. Pendry, "Negative refraction makes a perfect lens," *Phys Rev Lett*, vol. 85, no. 18, pp. 3966–3969, Oct. 2000, doi: 10.1103/PhysRevLett.85.3966.

[6] Y. Dong and T. Itoh, "Metamaterial-based antennas," in *Proceedings of the IEEE*, Institute of Electrical and Electronics Engineers Inc., 2012, pp. 2271–2285. doi: 10.1109/JPROC.2012.2187631.

[7] V. Pacheco-Peña and A. Yakovlev, "Computing with Square Electromagnetic Pulses," in *Handbook of Unconventional Computing, 1st ed., A. Adamatzky, Ed. World Scientific*, 2021, pp. 465–492. doi: 10.1142/9789811235740 0016.

[8] R. G. MacDonald, A. Yakovlev, and V. Pacheco-Peña, "Amplitude-Controlled Electromagnetic Pulse Switching Using Waveguide Junctions for High-Speed Computing Processes," *Advanced Intelligent Systems*, vol. 4, no. 12, p. 2200137, Dec. 2022, doi: 10.1002/aisy.202200137.

[9] A. Silva, F. Monticone, G. Castaldi, V. Galdi, A. Alù, and N. Engheta, "Performing mathematical operations with metamaterials," *Science (1979)*, vol. 343, no. 6167, pp. 160–163, 2014, doi: 10.1126/science.1242818.

[10] T. Knightley, A. Yakovlev, and V. Pacheco-Peña, "Neural Network Design of Multilayer Metamaterial for Temporal Differentiation," *Adv Opt Mater*, vol. 11, no. 5, Mar. 2023, doi: 10.1002/adom.202202351.

[11] D. A. Bykov, E. A. Bezus, L. L. Doskolovich, and V. A. Soifer, "Spatial integration and differentiation of optical beams in a slab waveguide by a dielectric ridge supporting high-Q resonances," *Opt Express*, vol. 26, no. 19, pp. 25156–25165, Sep. 2018, doi: 10.1364/OE.26.025156.

[12] N. M. Estakhri, B. Edwards, and N. Engheta, "Inverse-designed metastructures that solve equations," *Science (1979)*, vol. 363, no. 6433, pp. 1333–1338, 2019, doi: 10.1126/science.aaw2498.

[13] R. G. MacDonald, A. Yakovlev, and V. Pacheco-Peña, "Solving partial differential equations with waveguide-based metatronic networks," Dec. 2023, Accessed: Jan. 11, 2024. [Online]. Available: http://arxiv.org/abs/2401.00861

Investigating the variability of chorus waves in the radiation belts for improved understanding of nonlinear interactions

(Commission H submission)

Rachel Black* [1, 2], Oliver Allanson [3, 1], Nigel Meredith [2], and Andrew Hillier [1]
(1) University of Exeter, Exeter, United Kingdom; e-mail: rb894@exeter.ac.uk, a.hillier@exeter.ac.uk
(2) British Antarctic Survey, Cambridge, United Kingdom; e-mail: nmer@bas.ac.uk
(3) University of Birmingham, Birmingham, United Kingdom; o.d.allanson@bham.ac.uk

Earth's radiation belts can be described by two zones containing energetic charged particles; a more stable inner belt, and a highly dynamic outer belt. Wave-particle interactions have been identified as one of several processes responsible for the dynamics of electron populations within the outer region. Being able to describe these mechanisms is becoming increasingly important, given that the highest energy electrons present a risk to functioning satellites; the number of which is steadily growing. However, the dynamics of energetic electrons occur over many different time and length scales. This variability means that it is difficult to create a model capable of real-time prediction.

The most common method used by the international community for reproducing radiation belt dynamics involves Fokker-Planck diffusion models. Whilst, in many cases, these models effectively describe the global changes and interactions within the region, the Fokker-Planck approach depends upon a quasilinear theory. This assumes "small" wave amplitudes; however, recent observations have shown that this assumption may not always hold, with chorus waves being one of the most notable cases of high-amplitude waves. Accounting for this type of wave would require an extension of the modelling to include nonlinear effects.

Within two datasets of differing resolutions, the Van Allen Probe satellites provide multiple years' worth of information on the various waves and background fields inside the radiation belts. In this work, we present preliminary results of investigations comparing the lower resolution 'survey mode' data, with the high-resolution 'burst mode' data, captured during the mission. In particular, the work focusses on identifying chorus wave events in both datasets and assessing how the underlying variability may alter our interpretations of the wave properties. Utilising the higher resolution data in conjunction with the survey data allows closer inspection of the larger amplitude waves, and their potential implications for energetic electron dynamics in radiation belt modelling.

This paper's copyright is held by the author(s). It is published in these proceedings and included in any archive such as IEEE Xplore under the license granted by the "Agreement Granting URSI and IEICE Rights Related to Publication of Scholarly Work."

On the performance of plasmonic sensors enabled by Babinet's principle

J. A. Riley [(1),(2)], M. Horák[(3)] , R. G. Macdonald[(1),(2)], C. Johnson-Richards[(1)], N. Healy[(1)], V. Křápek[(3),(4)], and V. Pacheco-Peña[(1)]

1. *School of Mathematics, Statistics and Physics, Newcastle University, Newcastle Upon Tyne, NE1 7RU, United Kingdom.*
2. *School of Engineering, Newcastle University, Newcastle Upon Tyne NE1 7RU, UK*
3. *Central European Institute of Technology, Brno University of Technology, Purkyňova 123, 612 00, Brno, Czech Republic*
4. *Institute of Physical Engineering, Brno University of Technology, Technická 2, 616 69, Brno, Czech Republic*

Localized surface plasmons (LSPs) resonances in metallic micro-/nanostructures can enable subwavelength confinement of electromagnetic waves at optical wavelengths [1], [2]. LSPs have been used in diverse areas such as single particle fluorescence [3] and optical tweezers [4], among others, with applications to sensing devices also being proposed and demonstrated. This is due to the spectral position of LSPs being highly sensitive to variations near the plasmonic structures [5]. Observable spectral shifts occur, for example, as the refractive index of an adjacent dielectric changes. To facilitate the design of LSP structures, classical concepts have been applied to LSPs, such as the well-known Babinet's principle [2], [6], where complementary LSP modes are excited at similar spectral positions using plasmonic particles and their complementary versions (apertures) [7], [8]. It is important to note that at optical frequencies, metals are imperfect electric conductors causing slight differences to occur when applying Babinet's principle to plasmonics [6].

In this work, we present the design and experimental results of complementary cylindrical metallic particle- and aperture-dimers using Babinet's principle in plasmonics. The sensing performance of the complementary plasmonic structures is evaluated and compared by varying the refractive index of a dielectric film positioned atop them. A comprehensive exploration of their complementary nature and sensing performance will be discussed during the conference [9].

References

1. Stefan A. Maier, "Localized Surface Plasmons," in *Plasmonics: Fundamentals and Applications*, (New York, NY: Springer US, 2007), 65–88, doi:10.1007/0-387-37825-1_5.
2. V. Křápek et al., "Independent engineering of individual plasmon modes in plasmonic dimers with conductive and capacitive coupling," *Nanophotonics*, **9**, 3, 2020, pp. 623–632, doi:10.1515/nanoph-2019-0326.
3. A. Kinkhabwala et al., "Large single-molecule fluorescence enhancements produced by a bowtie nanoantenna," *Nature Photonics*, **3**, 11, 2009, pp. 654–657, doi:10.1038/nphoton.2009.187.
4. T. Shoji and Y. Tsuboi, "Plasmonic optical tweezers toward molecular manipulation: Tailoring plasmonic nanostructure, light source, and resonant trapping," *Journal of Physical Chemistry Letters*, **5**, 17, 2014, pp. 2957–2967, doi:10.1021/jz501231h.
5. B. B. Yousif and A. S. Samra, "Optical responses of plasmonic gold nanoantennas through numerical simulation," *Journal of Nanoparticle Research*, **15**, 1, 2013, pp. 1341, doi:10.1007/s11051-012-1341-3.
6. M. Horák et al., "Limits of Babinet's principle for solid and hollow plasmonic antennas," *Scientific Reports*, **9**, 1, 2019, pp. 1–11, doi:10.1038/s41598-019-40500-1.
7. M. Hrtoň et al., "Plasmonic Antennas with Electric, Magnetic, and Electromagnetic Hot Spots Based on Babinet's Principle," *Physical Review Applied*, **13**, 5, 2020, pp. 054045, doi:10.1103/PhysRevApplied.13.054045.
8. J. D. Ortiz et al., "Extension of Babinet's principle for plasmonic metasurfaces," *Applied Physics Letters*, **119**, 16, 2021, pp. 161103, doi:10.1063/5.0065724.
9. J. A. Riley et al., "Plasmonic sensing using Babinet's principle," *Nanophotonics*, 2023, pp. 53–56, doi:10.1515/nanoph-2023-0317.

Towards partial differential equation solvers using light-matter interactions

Ross Glyn MacDonald[1], **Alex Yakovlev**[2] **and Victor Pacheco-Peña**[1]

1. *School of Mathematics, Statistics and Physics, Newcastle University, Newcastle Upon Tyne, NE1 7RU, United Kingdom*
2. *School of Engineering, Newcastle University, Newcastle Upon Tyne, NE1 7RU, United Kingdom*

Electromagnetic (EM) wave based analogue computing has been proposed as a computing paradigm due to the intrinsic high-speed (computing at the speed of light in the medium) and potential for parallel computing[1]. In this realm, analogue EM wave-based processors have been reported to perform operations, such as differentiation, integration, and convolution[2–6]. In addition to this, comparably computationally intensive tasks, which require an iterative solving method by conventional computing techniques, have also been reported. For instance, ordinary differential equation[7], integral equation[8], and partial differential equation[9] (PDE) solving.

In regards to PDE solving, the introduction of metatronics[10] has allowed for electrical PDE solving techniques[11] to be implemented at higher frequencies. For instance, networks of metatronic elements embedded in epsilon-near-zero media[9], have been exploited to calculate solutions to the Poisson equation. Inspired by the potential applications of metatronic circuits for high-speed analogue computing. In this work, we present a method of using waveguide-based metatronic circuits to calculate solutions to PDEs in the form of the Helmholtz equation[12]. To do this we exploit a network of waveguide-based metatronic circuits emulating electrical T-circuits connected in series[13–15]. Theoretical and numerical results of the magnetic field distribution will be presented, for the structure solving a range of Dirichlet and open boundary value problems.

References

1. Zangeneh-Nejad, F., Sounas, D. L., Alù, A. & Fleury, R. Analogue computing with metamaterials. *Nat. Rev. Mater.* **6**, 207–225 (2020).
2. Silva, A. *et al.* Performing Mathematical Operations with Metamaterials. *Science (80-.).* **343**, 160–163 (2014).
3. Sol, J., Smith, D. R. & del Hougne, P. Meta-programmable analog differentiator. *Nat. Commun.* **13**, 1713 (2022).
4. Zhu, T. *et al.* Plasmonic computing of spatial differentiation. *Nat. Commun.* **8**, 15391 (2017).
5. Momeni, A., Rouhi, K. & Fleury, R. Switchable and simultaneous spatiotemporal analog computing with computational graphene-based multilayers. *Carbon N. Y.* **186**, 599–611 (2022).
6. MacDonald, R. G., Yakovlev, A. & Pacheco-Peña, V. Time derivatives via interconnected waveguides. *Sci. Rep.* **13**, 13126 (2023).
7. Zangeneh-Nejad, F. & Fleury, R. Topological analog signal processing. *Nat. Commun.* **10**, 2058 (2019).
8. Mohammadi Estakhri, N., Edwards, B. & Engheta, N. Inverse-designed metastructures that solve equations. *Science (80-.).* **363**, 1333–1338 (2019).
9. Miscuglio, M. *et al.* Approximate analog computing with metatronic circuits. *Commun. Phys.* **4**, 196 (2021).
10. Engheta, N. Circuits with Light at Nanoscales: Optical Nanocircuits Inspired by Metamaterials. *Science (80-.).* **317**, 1698–1702 (2007).
11. Save, Y. D., Narayanan, H. & Patkar, S. B. Solution of Partial Differential Equations by electrical analogy. *J. Comput. Sci.* **2**, 18–30 (2011).
12. MacDonald, R. G., Yakovlev, A. & Pacheco-Peña, V. Solving partial differential equations with waveguide-based metatronic networks, arXiv:2401.00861 (2023).
13. Yakovlev, A. & Pacheco-Peña, V. Enabling High-Speed Computing with Electromagnetic Pulse Switching. *Adv. Mater. Technol.* **5**, 2000796 (2020).
14. Pacheco-Peña, V. & Yakovlev, A. Computing with Square Electromagnetic Pulses. in *Handbook of Unconventional Computing,* (ed. Adamatzky, A.) 465–492 (World Scientific, 2021). doi:10.1142/9789811235740_0016.
15. MacDonald, R. G., Yakovlev, A. & Pacheco-Peña, V. Amplitude-Controlled Electromagnetic Pulse Switching Using Waveguide Junctions for High-Speed Computing Processes. *Adv. Intell. Syst.* **2200137**, 2200137 (2022).

Electromagnetic properties of additive manufactured polymers at telecommunication wavelengths

Joseph Arnold Riley [(1),(2)], Christian Johnson-Richards[(1)], Noel Healy[(1)], and Victor Pacheco-Peña[(1)]

1. *School of Mathematics, Statistics and Physics, Newcastle University, Newcastle Upon Tyne, NE1 7RU, United Kingdom.*
2. *School of Engineering, Newcastle University, Newcastle Upon Tyne NE1 7RU, UK*

The rapid expansion of the field of photonics has enabled an astonishing amount of ground-breaking applications such as optical spectroscopy and sensing [1], metamaterials [2] and optical computing [3]. At telecommunication wavelengths, commonly used materials include Silicon (Si) and Germanium (Ge) given that they have high refractive index and low losses, enabling them to produce compact and efficient photonic devices [4], [5]. Recently, additive manufacturing processes have grown in popularity given that they can enable rapid prototyping and low-cost fabrication. Interestingly, polymers have been proposed as materials for photonic applications including sensors and waveguides [6]. Here, we will discuss our recent efforts in studying alternative materials for photonic applications by experimentally characterising the electromagnetic properties (complex refractive index) at telecommunication wavelengths of four commercially available 3D printable polymers, namely: polylactic acid (PLA), recycled polyethylene terephthalate (rPET), rPLA, and butene-diol vinyl alcohol (BVOH). Their complex refractive index is obtained within the telecom wavelength range of 1520 - 1630 nm [7]. It will be shown how they offer a promising alternative for 3D printed telecom photonic devices with low losses. Moreover, the chosen materials present important technological and societal attributes such as renewability, recyclability, or water solubility [8].

References

[1] Q. Liu, “Role of optical spectroscopy using endogenous contrasts in clinical cancer diagnosis,” *World J. Clin. Oncol.*, vol. 2, no. 1, p. 50, 2011, doi: 10.5306/wjco.v2.i1.50.

[2] T. Knightley, A. Yakovlev, and V. Pacheco-Peña, “Neural Network Design of Multilayer Metamaterial for Temporal Differentiation,” *Adv. Opt. Mater.*, vol. 2202351, p. 2202351, Dec. 2022, doi: 10.1002/adom.202202351.

[3] R. G. MacDonald, A. Yakovlev, and V. Pacheco-Peña, “Amplitude-Controlled Electromagnetic Pulse Switching Using Waveguide Junctions for High-Speed Computing Processes,” *Adv. Intell. Syst.*, vol. 4, no. 12, Dec. 2022, doi: 10.1002/aisy.202200137.

[4] Y. Shi *et al.*, “Silicon photonics for high-capacity data communications,” *Photonics Res.*, vol. 10, no. 9, p. A106, 2022, doi: 10.1364/prj.456772.

[5] V. Reboud *et al.*, “Germanium based photonic components toward a full silicon/germanium photonic platform,” *Prog. Cryst. Growth Charact. Mater.*, vol. 63, no. 2, pp. 1–24, 2017, doi: 10.1016/j.pcrysgrow.2017.04.004.

[6] S. N. Khonina, G. S. Voronkov, E. P. Grakhova, N. L. Kazanskiy, R. V. Kutluyarov, and M. A. Butt, “Polymer Waveguide-Based Optical Sensors—Interest in Bio, Gas, Temperature, and Mechanical Sensing Applications,” *Coatings*, vol. 13, no. 3, 2023, doi: 10.3390/coatings13030549.

[7] J. A. Riley, C. Johnson-Richards, N. Healy, and V. Pacheco-Peña, “Refractive index retrieval of 3D printed materials for photonic applications at telecom wavelengths,” *Prep.*, 2024.

[8] D. Yu *et al.*, “Structure and properties of polylactic acid/butenediol vinyl alcohol copolymer blend fibers,” *Int. J. Biol. Macromol.*, vol. 232, no. January, p. 123396, 2023, doi: 10.1016/j.ijbiomac.2023.123396.

Scattering Matrix Evaluation of a 6-port Valley Photonic Crystal

Christian Johnson-Richards[1], **Alex Yakovlev**[2] **and Victor Pacheco-Peña** [1]

1. *School of Mathematics, Statistics and Physics, Newcastle University, Newcastle Upon Tyne, NE1 7RU, United Kingdom;*
2. School of Engineering, Newcastle University, Newcastle Upon Tyne, NE1 7RU, United Kingdom

Valley photonic crystals (VPCs) have shown to enable the design of photonic waveguides including sharp bends [1] with low-loss [2], [3] and unidirectional transport [4]. For this, it is required to design a lattice with hexagonal unit cells and with a broken inversion symmetry. A topological waveguide can then be formed by aligning two VPCs with opposing valley-Chern numbers [5]. There is a broad range of applications of VPCs including optical logic operations [6], routing [3] and quantum computing [7]. In order to enable efficient coupling between junctions in large $N \times N$ networks of VPC junctions, one can design individual rotationally symmetric junctions that can form seamless interconnects. This can be achieved by, for instance, designing a rotationally symmetric 6-port junction with 6 identical waveguides [8], [9]. importantly, it has recently been demonstrated that scattering parameters can be numerically extracted from VPC-based interconnected waveguides [10]. In this communication we will discuss our recent efforts in applying VPCs to computing application with light [11]. A 6-port VPC junction will be discussed with the ability to enable equal power division to three output ports, with almost zero reflection. A detailed discussion into the extraction of a scattering matrix that defines the proposed structure will also be presented, showing how the proposed structure could be used for applications such as wave director.

References

[1] J. K. Yang, Y. Hwang, and S. S. Oh, “Evolution of topological edge modes from honeycomb photonic crystals to triangular-lattice photonic crystals,” *Phys. Rev. Res.*, vol. 3, no. 2, pp. 1–6, 2021, doi: 10.1103/PhysRevResearch.3.L022025.

[2] Z. Qi *et al.*, “Electrical tunable topological valley photonic crystals for on-chip optical communications in the telecom band,” *Nanophotonics*, vol. 11, no. 18, pp. 4273–4285, 2022, doi: 10.1515/nanoph-2022-0169.

[3] X.-T. He *et al.*, “A silicon-on-insulator slab for topological valley transport,” *Nat. Commun.*, vol. 10, no. 1, p. 872, 2019, doi: 10.1038/s41467-019-08881-z.

[4] B. L. Li *et al.*, “Valley topological line-defects for Terahertz waveguides and power divider,” *Opt. Mater. (Amst).*, vol. 126, no. February, p. 112152, 2022, doi: 10.1016/j.optmat.2022.112152.

[5] D. Bisharat, R. Davis, Y. Zhou, P. Bandaru, and D. Sievenpiper, “Photonic Topological Insulators: A Beginner’s Introduction [Electromagnetic Perspectives],” *IEEE Antennas Propag. Mag.*, vol. 63, no. 3, pp. 112–124, 2021, doi: 10.1109/MAP.2021.3069276.

[6] M.-H. Chao, B. Cheng, Q.-S. Liu, W.-J. Zhang, Y. Xu, and G.-F. Song, “Novel optical XOR/OR logic gates based on topologically protected valley photonic crystals edges,” *J. Opt.*, vol. 23, no. 11, p. 115002, Oct. 2021, doi: 10.1088/2040-8986/ac11ac.

[7] Y. Chen *et al.*, “Topologically Protected Valley-Dependent Quantum Photonic Circuits,” *Phys. Rev. Lett.*, vol. 126, no. 23, p. 230503, Jun. 2021, doi: 10.1103/PhysRevLett.126.230503.

[8] T. Hou, Y. Ren, Y. Quan, J. Jung, W. Ren, and Z. Qiao, “Valley current splitter in minimally twisted bilayer graphene,” *Phys. Rev. B*, vol. 102, no. 8, pp. 1–6, 2020, doi: 10.1103/PhysRevB.102.085433.

[9] R. Zheng *et al.*, “Topological network transport in on-chip phononic crystals,” *Phys. Rev. B*, vol. 107, no. 24, p. 245122, 2023, doi: 10.1103/PhysRevB.107.245122.

[10] G. Lévêque *et al.*, “Scattering-matrix approach for a quantitative evaluation of the topological protection in valley photonic crystals,” *Phys. Rev. A*, vol. 108, no. 4, p. 43505, Oct. 2023, doi: 10.1103/PhysRevA.108.043505.

[11] C. Johnson-Richards, A. Yakovlev, and V. Pacheco-Peña, “Topological Valley Photonic Waveguides: Scattering matrix evaluation for linear computing,” *Prep.*, 2024.

Statistics of Small-Scale Ionospheric Waves in European Mid-Latitudes Observed Using LOFAR

Ben Boyde*[1], Alan G. Wood[1], Gareth Dorrian[1], Francesco de Gasperin[2][3], Frits Sweijen[4], Maaijke Mevius[5], and Kasia Beser[5]

(1) Space Environment and Radio Engineering, School of Engineering, University of Birmingham, Edgbaston, B15 2TT, Birmingham, UK

(2) INAF - Istituto di Radioastronomia, Via P. Gobetti 101, 40129 Bologna, Italy

(3) Hamburger Sternwarte, University of Hamburg, Gojenbergsweg 112, 21029 Hamburg, Germany

(4) Leiden Observatory, Leiden University, P.O. Box 9513, 2300 RA Leiden, The Netherlands

(5) ASTRON – The Netherlands Institute for Radio Astronomy, Oude Hoogeveensedijk 4, 7991 PD Dwingeloo, The Netherlands

The LOw Frequency ARray (LOFAR) is a radio telescope centred in the Netherlands, consisting of over 50 individual stations. The observed impact of the ionosphere on signals from astronomical radio sources can be used to derive differential Total Electron Content (dTEC) between the lines of sight from different LOFAR stations. The dTEC derived in calibration has extremely high precision (~ 1 mTECu) and is available at high temporal (~ 4 s) and spatial (baselines from ~ 100 m to ~ 100 km) resolutions. This is routinely calculated for astronomical observations as part of the calibration process required to mitigate instrumental and ionospheric distortions to the images, however this data is not currently widely available or used within the ionospheric community. These measurements provide a new means of studying ionospheric disturbances in the mid-latitudes.

A method for identifying wave signatures in the dTEC data has been developed and shown to be capable of identifying waves with amplitudes as low as a few mTECu [1]. This method has been used to analyse over 2,500 hours of observations made as part of an astronomical survey. The statistical characteristics of the identified waves and their dependence on time of day, season, and geomagnetic activity are discussed, such as variations in dominant propagation direction. Potential source mechanisms, both terrestrial (e.g. convective systems, solar terminator) and space weather (e.g. auroral activity) are considered to explain the observed characteristics. These observations extend the range of ionospheric waves that can be identified to shorter wavelengths and lower amplitudes beyond what is currently detectable using GNSS derived TEC. This method complements established techniques for detecting ionospheric waves.

References

[1] B. Boyde, A. G. Wood, G. Dorrian, F. Sweijen, F. de Gasperin, M. Mevius, K. Beser, D. Themens, "Wavelet Analysis of Differential TEC Measurements Obtained Using LOFAR," Radio Science (Under Review), 2023, doi: 10.22541/essoar.169754969.93126117/v1

URSI UK Symposium, 21 February 2024

Understanding Supermassive Black Hole Outflows with International LOFAR

James Petley*(1) and Leah Morabito(1)
(1) Centre for Extragalactic Astronomy, Durham University; e-mail: james.w.petley@durham.ac.uk

1 Extended Abstract

Quasars are some of the most luminous sources in the universe and are powered by the accretion of matter onto supermassive black holes at the center of galaxies. These sources have produced some of the most awe-inspiring images in astronomy. Unfortunately, most radio-detected quasars do not display such impressive features, they are fainter and more compact, and we need to leverage the latest developments in VLBI radio astronomy to study their physics in detail.

Around 10-20% of quasar spectra exhibit massive gas outflow features in their spectra. These quasars are known as Broad Absorption Line Quasars (BALQSOs) [1]. Previous studies of BALQSOs have found a puzzling connection to radio emission: BALQSOs are more likely to be radio-detected than other quasars but BALQSOs are still more likely to be "radio-quiet" than other quasars [2]. Most recently this was investigated in [3] where we showed that the shape of the wind signatures is also connected to radio emission. However, the physical origin of the radio emission is still not decided.

We are undertaking an ambitious project to study BALQSOs, utilising the International LOFAR Telescope, which will form part of a larger sky survey. We combine this data with observations from e-MERLIN, another VLBI instrument, for the brightest 10 sources. e-MERLIN operates at a higher frequency but at the same resolution allowing for complementary spectral data which may help to determine the source of radio-emission.

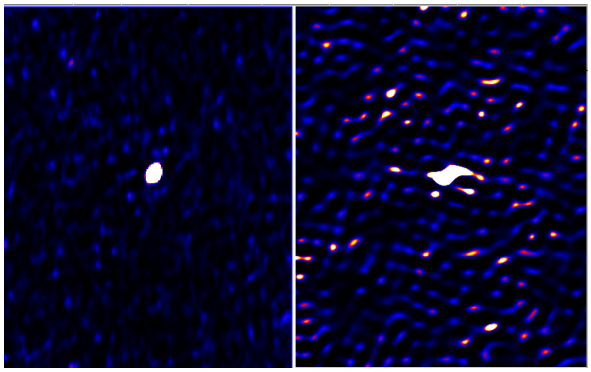

Figure 1. BALQSO image from the International LOFAR Telescope (left) and eMERLIN (right). These instruments have the same resolution despite an order of magnitude difference in frequency.

References

[1] R. J. Weymann et al., "Comparisons of the Emission-Line and Continuum Properties of Broad Absorption Line and Normal Quasi-stellar Objects", *The Astrophysical Journal*, **373**, May 1991, p. 23, doi: 10.1086/170020

[2] L. K. Morabito et al., "The origin of radio emission in broad absorption line quasars: Results from the LOFAR Two-metre Sky Survey", *Astronomy and Astrophysics*, **622**, A15, February 2019, p.17, doi:10.48550/arXiv.1811.07931

[3] J. W. Petley et al., "Connecting radio emission to AGN wind properties with broad absorption line quasars", *Monthly Notices of the Royal Astronomical Society*, **515**, 4, October 2022, pp.5159-5174, doi:10.48550/arXiv.2207.10102

Falls Risk Screening with Millimetre-Wave Radar

Elif Dogu[1], Jose A. Paredes[2], Akram Alomainy[1], Janelle M. Jones[3] and Khalid Z. Rajab[1]

The incidence of falls in the older adults is a worldwide health problem, requiring innovative methods to screen for the risk of falls promptly and efficiently. Falls risk screening is the first step of the falls risk assessment and prevention process [1]. The American Geriatrics Society and British Geriatrics Society both recommend that all adults over the age of 65 should be screened for falls risk at least once a year [2]. However, effective falls risk screening is still underutilised and not routinely integrated into clinical practice [3]. There might be several reasons such as constraints of clinical time and environment. Radar technology can be a promising solution to automate these procedures, with its capabilities such as recognising activities [4] and capturing gait parameters [5]. This study explores the integration of millimetre-wave radar technology with the Timed Up and Go (TUG) test, which is a widely used falls risk screening tool that combines parameters measuring a person's dynamic balance and functional mobility. Frequency Modulated Continuous Wave (FMCW) radar is used to assess the performance against video recordings in TUG completion time measurement. The completion time is inferred from radar measurements with two different methods based on distance and micro-Doppler (i.e. velocity). The TUG completion time inferred from the distance measurements of radar has achieved a level of accuracy (3.48% error, 0.9996 correlation) surpassing that of manual timing (4.26% error, 0.9960 correlation). Although micro-Doppler timings were less accurate than distance (6.49% error, 0.9936 correlation), due to the radar's high sensitivity in detecting small movements, both techniques had sufficient performance to satisfy the requirements set by healthcare professionals. This suggests a viable and effective incorporation of radar technology into falls risk screening protocols.

References

[1] M. Montero-Odasso *et al.*, 'World guidelines for falls prevention and management for older adults: a global initiative', *Age and Ageing*, vol. 51, no. 9, p. afac205, Sep. 2022, doi: 10.1093/ageing/afac205.

[2] L. V. V. Moncada, 'Management of Falls in Older Persons: A Prescription for Prevention', *American Family Physician*, vol. 84, no. 11, pp. 1267–1276, Dec. 2011.

[3] R. Sun and J. J. Sosnoff, 'Novel sensing technology in fall risk assessment in older adults: a systematic review', *BMC Geriatr*, vol. 18, no. 1, p. 14, Jan. 2018, doi: 10.1186/s12877-018-0706-6.

[4] K. Z. Rajab, B. Wu, P. Alizadeh, and A. Alomainy, 'Multi-target tracking and activity classification with millimeter-wave radar', *Applied Physics Letters*, vol. 119, no. 3, p. 034101, Jul. 2021, doi: 10.1063/5.0055641.

[5] J. Ayena, L. Chioukh, M. Otis, and D. Deslandes, 'Risk of Falling in a Timed Up and Go Test Using an UWB Radar and an Instrumented Insole', *Sensors*, vol. 21, no. 3, Feb. 2021, doi: 10.3390/s21030722.

[1] School of Electronic Engineering and Computer Science, Queen Mary University of London, London E1 4NS, United Kingdom

[2] School of Arts, Humanities and Social Sciences, University of Roehampton, London SW15 5PU, United Kingdom

[3] School of Biological and Behavioural Sciences, Queen Mary University of London, London E1 4NS, United Kingdom

USRI Proposal

Non-destructive identification of archeological objects using resonant cavity perturbation technique

Isabella Langdon and Martin Robinson, University of York, UK

Introduction

In the field of archeology there is a pressing need for non-destructive identification methods. Historically, and indeed up to the present era, testing on archeological artifacts has been destructive in nature. This abstract introduces an innovative new technique, invented by Dr Martin Robinson and developed by PhD student Isabella Langdon, employs resonant cavity perturbation (RCP) for the non-destructive identification of archeological objects. This method stands out, due to its ability to accurately differentiate between dielectric materials without damaging artifacts.

Methodology

RCP has existed as a technique for decades, but historically its use has been limited by the shape requirements of the object being studied. This limitation is caused by the q-factor and frequency of the results being tied to shape, traditionally this is solved by milling or casting the object into a disc. Our novel technique instead compares the artifact against a 3D printed replica, or simulation, of which the material is known. By testing both original and replica to each other, we can eliminate shape dependency, giving us the loss factor and the permittivity.

What we have done

An initial version of the machine was built, colloquially known as “4M”. Testing was conducted with 3D replicas of the original, which found the machinery was capable of telling apart objects of very close composition, although a fault was found that made the machinery unable to distinguish objects that were not 90* rotationally symmetrical.

What we are doing

To solve the issue found in 4M, and to improve accuracy and speed of measurement, we have built 4M 2.0. Version 2 should solve the issue of shape dependency that was found in the previous version, as well as improving accuracy by decreasing chamber size and improving software. We have also replaced the 3D printing aspect with a simulated version using CST.

Applications

The most prominent application for this novel technique is its use in the reassembly of Ashurbanipal’s Library, one of the oldest surviving libraries in the world. Our method facilitates the sorting of the some 30,000 fragments that comprise the collection based on their origin, showcasing its practical utility in solving complex archeological tasks.

Comparative Analysis

We plan to compare our results to those gathered by pXRF, another technique that is nondestructive. There are fundamental differences between 4M and pXRF, namely the depth of their scanning, and the results taken. Nevertheless, we believe that pXRF, having been in use by the archeological community for the past 15 years, makes a good comparative technique to help verify our own results.

Optimized Design of a Compact Rectangular Metamaterial Sensor for Bone Fracture Detection

Prince O. Siaw[1], Mohamed Lashab[2], Ebenezer Adjei[1], Ahmad Aldelemy[1], Raed A. Abd-Alhameed[1]

[1]Fculty of Engineering and Informatics, University of Bradford,United, Kingdom
[2]Department of Electronics, University ofOum El Bouagui, Oum El Bouagui,Algeria

p.o.siaw@bradford.ac.uk[1], Lashabmoh@gmail.com[2], e.adjei@bradford.ac.uk[1], a.a.aldelemy@bradford.ac.uk[1]r.a.a.abd@bradford.ac.uk[1],

Wireless communication technologies have enabled health monitoring applications, notably body-centric systems. These devices' metamaterial sensors may detect bone fractures. They are vital antennae for body gadgets and external networks. These sensors respond to electromagnetic waves flowing through biological tissues and are very sensitive to material changes to detect fractures [1].

When a bone breaks, its physical properties change, affecting its electromagnetic wave interaction. Metamaterial sensors detect these changes and send the data to a receiver, which evaluates it for fractures. However, human closeness to the antenna reduces radiation efficacy, affecting pattern and gain. Electromagnetic radiation in human tissues reduces radiation efficacy for body-centric applications [2,3]

A 0.80mm FR-4 substrate was used to simulate and build the proposed antenna in the CST microwave studio. The suggested antenna is 40.00 mm2 x 24.00 mm^2, as indicated in figures 1&2. The suggested antenna's bandwidth, gain, efficiency, and radiation pattern are examined. Our results indicate that the suggested antenna retains its bandwidth whether in close contact with the human body or artificial femur phantom.

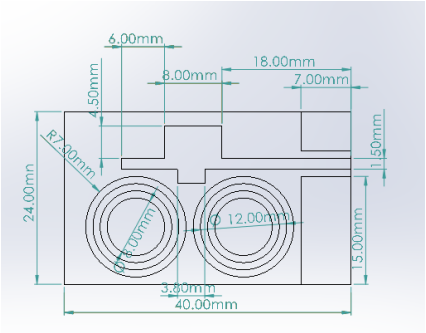

Fig.1 antenna geometry model

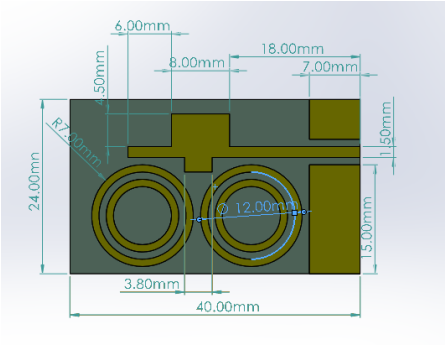

Fig.2. Prototype of the proposed antenna

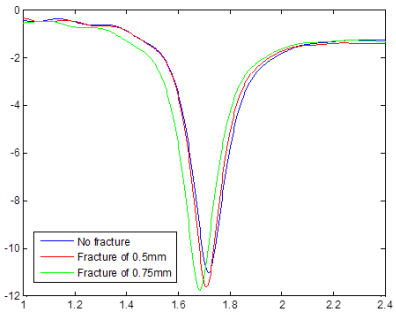

Fig.3. Simulated and measured results

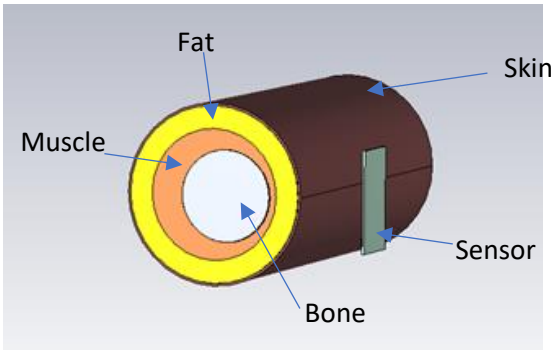

Fig.4. Body phantom model with the proposed antenna

References:

[1] R. Melik et al., "Nested Metamaterials for Wireless Strain Sensing," in IEEE Journal of Selected Topics in Quantum Electronics, vol. 16, no. 2, pp. 450-458, March-april 2010, doi: 10.1109/JSTQE.2009.2033391.

[2] Kunal Kumar Singh, Santosh Kumar Mahto and Sinha, R. (2023). A review: material characterization with metamaterial-based sensors. Sensor Review, 43(2), pp.41–51. doi:https://doi.org/10.1108/sr-09-2021-0325.

[3] Alhameed, R.A. (2023). 'Exploring Radio Frequency Techniques for Bone Fracture Detection: A Comprehensive Review of Low Frequency and Microwave Approaches'. 10(1). doi:https://doi.org/10.19080/arr.2023.10.555778.

Understanding spectral artefacts in SKA-LOW 21-cm cosmology experiments: the impact of cable reflections.

Oscar Sage David O'Hara[1,2], Fred Dulwich[1,2], Jiten Dhandha[2,3], Thomas Gessey-Jones[1,2], Anastasia Fialkov[2,3], Eloy de Lera Acedo[1,2]

[1] Cavendish Astrophysics, University of Cambridge, Cambridge, CB3 0HE, UK
[2] Kavli Institute for Cosmology in Cambridge, University of Cambridge, Cambridge, CB3 0HA, UK
[3] Institute of Astronomy, University of Cambridge, Cambridge, CB3 0HA, UK

The Aperture Array Verification System 2 is an engineering platform array for the Square Kilometer Array (SKA), featuring 7m coaxial transmission lines connecting the low noise amplifier of the SKALA4.1 antenna to the SMART box. An impedance mismatch between these components results in a partially reflected electromagnetic signal, which introduces chromatic aberrations in the instrument bandpass, and propagates the foreground power to higher delays, potentially contaminating the Epoch of Reionisation (EoR) Window. This talk presents an end-to-end simulation pipeline for SKA-LOW based on the Oxford Square Kilometre Array Simulator using a composite sky model that combines radio foregrounds from The Galactic and Extragalactic All-Sky MWA Survey, Haslam 408MHz, and a simulated 1.5cGpc 21-cm brightness temperature cube generated via a semi-numerical code, 21cmSPACE. We implement a parametric approach to account for the effects of the coaxial transmission line and derive an analytical model that expresses the scattering parameters in terms of the bulk material parameters and is consistent with numerical simulation to 5%. The delay power spectrum is subdivided into The Foreground Wedge and two k-mode regions of The EoR Window, those with suppressed foreground emission and those dominated by supra-horizon emission, to quantify potentially contaminated k-modes in a statistically significant manner. We demonstrate that a coaxial transmission line of length ≤ 15.0m with an impedance mismatch ≤ 10Ω and thus SKA-LOW, will not prevent a successful detection of the 21cm signal within the EoR Window. However, experiments that implement foreground removal must be trained with prior knowledge of the cable specifications, tolerances and thermal variation.

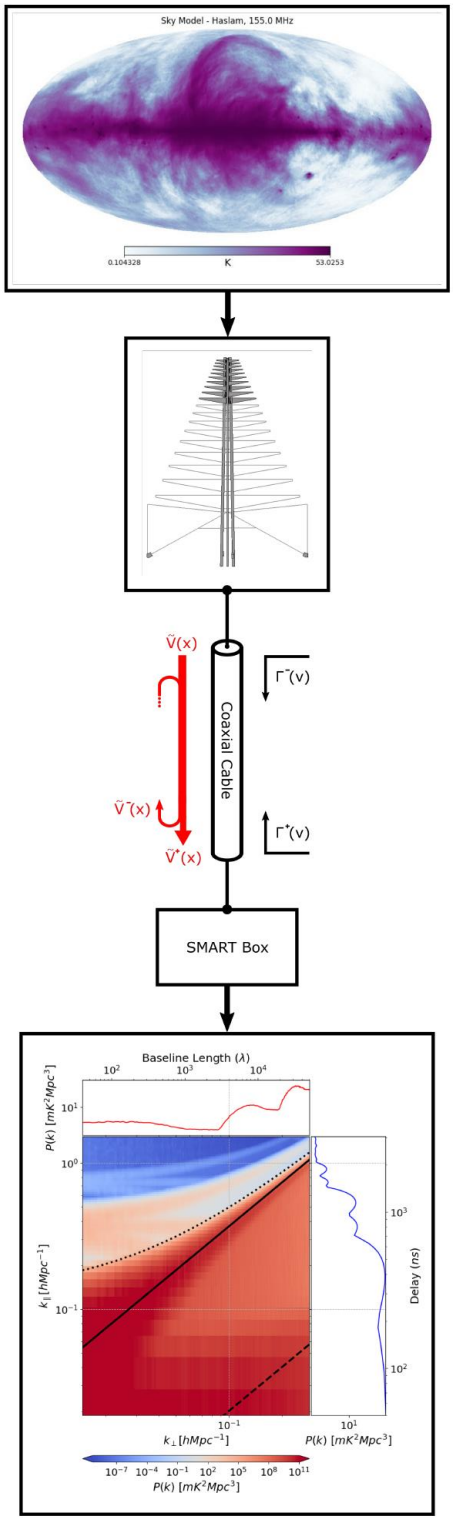

Figure 1. For SKA-LOW, the interferometric response of each SKALA element will propagate from the low-noise amplifier (LNA) as an electrical signal along a coaxial transmission line towards the SMART boxes for long-range transmission to the beamformer. If an impedance mismatch is observed between the front-end components and the transmission line the signal will experience a partial reflection. As a result of these reflections smooth radio foregrounds typically confined below the horizon limit are pushed to higher delays contaminating the EoR window.

Title

Reconfigurable Intelligent Surfaces (RISs) Assisted Non-Terrestrial Networks (NTNs) based 6G Communications

Chika Worka, University of Huddersfield

Event Details

Event: 2024 URSI UK Symposium
Date: Wednesday 21 February 2024
Location: UK National Physical Laboratory, Teddington

Commission C Focus: Radio communication Systems and Signal Processing

Abstract: The evolution of Non-Terrestrial Networks (NTNs) from 5G to 6G demands innovative solutions to address the increasing density of mobile users, the surge in mobile data traffic, and diverse service requirements. High-frequency electromagnetic waves, integral to these NTN environments, face obstacles and distance limitations. Reconfigurable Intelligent Surfaces
(RISs) have emerged as a promising technology, dynamically enhancing wireless network capacity and coverage in NTNs by modifying the wireless propagation environment. Positioned as potential contributor to the sixth generation of communication networks in NTNs, RISs offer solutions to overcome existing challenges. Machine Learning (ML) stands out as an effective approach for optimizing RIS-assisted communication systems in NTN scenarios, particularly as computational complexity increases with user-infrastructure interactions. This paper thoroughly investigates ML algorithms in the context of RISs within NTNs, providing an overview of RIS technology, summarizing ML methods applied to RIS architecture, and comparing various methodologies.

Keywords: Non-Terrestrial Networks (NTNs), Machine Learning (ML), Reconfigurable Intelligent Surfaces (RISs), Low-Earth Orbit (LEO) satellite communication.

Radio-mode feedback in high-redshift galaxy clusters with the International LOFAR Telescope

Roland Timmerman, Durham University

Abstract: As the intracluster medium (ICM) in galaxy clusters cools through the emission of X-ray radiation, it sinks down toward the central galaxy where it fuels the AGN. This AGN subsequently produces radio-mode feedback in the form of powerful jets of relativistic plasma which re-energize the ICM, completing the feedback cycle. Measurements of the energy injected by radio-mode feedback into the cluster environment have mostly relied on X-ray observations, which reveal cavities in the ICM excavated by the radio lobes. However, the sensitivity required to accurately constrain the dimensions of these cavities has proven to be a major limiting factor, and forms the main bottleneck on high-redshift ($z > 0.6$) measurements. Recent developments by Timmerman et al. (2022) opened a new observational window on radio-mode feedback by demonstrating that low-frequency radio observations taken with the International LOFAR Telescope (ILT) provide the combination of sensitivity and resolution required to reliably map the radio lobes in detail. This resolves the primary bottleneck experienced with X-ray observations and enables radio-mode feedback studies toward the high-redshift regime for the first time. In this talk, we explain this method for measuring the amount of radio-mode feedback in galaxy clusters and present the first results of applying this method using ILT observations on a sample of galaxy clusters at $z > 0.6$.

Title

Building a reliable THz material library

Authors

Dou Feng, Christopher Sumner, Morgan Dryhurst, Jie Qing, Olcay Altıntaş, Aleksandr Bystrov and Miguel Navarro-Cía

Abstract

Compared to the millimeter wave and SHF microwave, the huge bandwidth available at TeraHertz (THz) frequency makes it attractive for future data transmission and networking use. Although THz frequency signals are highly absorbed by the gases of the atmosphere, they are still very promising for high-bandwidth wireless networking systems, especially indoor systems. This report analyzed the material characterization of around hundred common indoor materials which can be classified as fabric, leather, wood, stone and plastics by using THz Time Domain Spectroscopy technique. Materials were measured with Toptica TeraFlash Pro Dual in both collimated and focused beam transmission configuration and then analyzed using the commercial software Teralyzer to acquire properties of refraction index, absorption coefficient, permittivity, and loss tangent. The results at 0.3 and 0.45THz are singled-out and further analyzed given the prospect of these frequencies for future 6G communication. An intercomparison of the results from Toptica TeraFlash Pro Dual, Menlo Tera K15 and Keysight N5247B PNA-X with VDI extenders was carried out to understand the influence of the system in the material extraction process and build up a reliable material library.

Real-time Monitoring of Femur Fractures with AI-enhanced RF Sensors

Ahmad Aldelemy, Prince O. Siaw, Ebenezer Adjei, Raed A. Abd-Alhameed[1]
Faculty of Engineering and Informatics, University of Bradford, United, Kingdom
a.a.aldelemy@bradford.ac.uk[1] , p.o.siaw@bradford.ac.uk[1], e.adjei@bradford.ac.uk[1], r.a.a.abd@bradford.ac.uk[1],

Femur fractures are a common orthopaedic injury, according to a study conducted by the GBD 2019 Fracture Collaborators, there were 178 million new fractures globally in 2019, which is a 33.4% increase since 1990. The number of people living with fracture-related disabilities also rose by 65.3% during this period 12 [1]. The healing process of femur fractures is complex and can be challenging to monitor. Traditional methods, such as physical examination and radiographic imaging, can provide valuable information, but they are limited in their ability to provide real-time, detailed insights.[2]. This research introduces a ground-breaking approach that leverages Radio Frequency (RF) sensors and Artificial Intelligence (AI) to revolutionise real-time femur fracture monitoring, potentially transforming patient care and orthopaedic diagnostics.

RF sensors offer a non-invasive method to monitor the healing of fractures by detecting changes in the dielectric properties of bone. While they provide valuable data, it's important to note that they complement rather than replace traditional imaging methods like X-rays. These sensors add a continuous monitoring dimension, which may capture certain aspects of healing not visible in intermittent imaging.[3].

Integrating AI with RF sensor data enables precise identification of bone healing stages and offers real-time insights for clinicians. This aids in the early detection of healing issues, informs personalised rehabilitation plans, and helps predict healing outcomes, enhancing patient care and reducing complications.

This technology advances patient care by enabling continuous bone healing monitoring, which offers a comprehensive understanding of recovery and identifies any irregularities promptly. It also reduces patient discomfort by decreasing the need for repeated X-rays and lowers radiation exposure. Moreover, access to immediate and precise data supports clinicians in making well-informed decisions and tailoring treatment plans to individual patient needs.

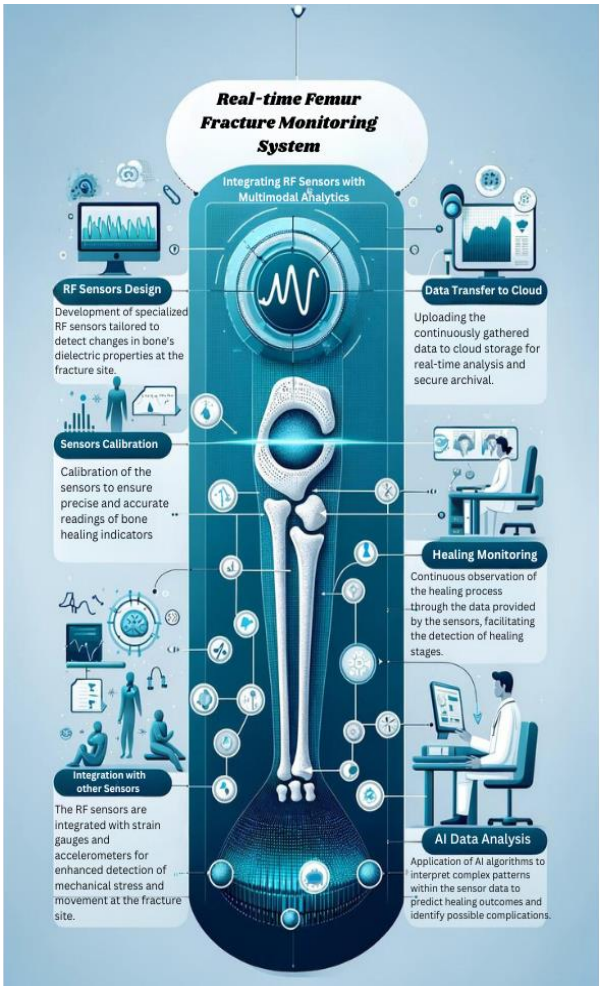

Initial simulations of a system for femur fracture management have shown promising results in distinguishing healing stages through distinct RF signal patterns, outperforming conventional methods in sensitivity and specificity. The system's ability to distinguish healing stages could potentially enhance femur fracture management by providing more accurate diagnoses and treatment plans. As the simulations progress, we hope to see even better results that could revolutionise the way femur fractures are managed. This approach holds immense potential to improve patient outcomes, reduce healthcare costs, and transform orthopaedics by enabling personalised, data-driven care.

References

1. The global burden of fractures, The Lancet Healthy Longevity, ISSN: 2666-7568, Vol: 2, Issue: 9, Page: e535-e536, 2021, DOI10.1016/s2666-7568(21)00183-5
2. National Research Council of Italy (CNR). 'The Dielectric Properties of Body Tissues'. Available at: http://niremf.ifac.cnr.it/docs/DIELECTRIC/Report.html.
3. Ahmad Aldelemy and et al, Exploring Radio Frequency Techniques for Bone Fracture Detection: A Comprehensive Review of Low Frequency and Microwave Approaches, Ann Rev Research 10(1): ARR.MS.ID.555778 (2023), pp. 1-21, DOI: 10.19080/ARR.2023.10.555778

Shielding Effectiveness of Reverberant Equipment Enclosures Measured in Reverberation Chamber

Ali Ghaffarlouy Raef, Professor Andy Marvin, Dr. Martin Robinson, Dr. Simon Bale, and Dr. John Dawson

University of York - School of Physics, Engineering, and Technology

The unwanted influence of electromagnetic waves on electronic devices or systems can originate from various sources. When these waves interact with susceptible electronic components, they can induce unwanted currents or voltages, disrupting normal operation and potentially causing malfunctions. The shielding effectiveness (SE) of an enclosure is a measure of how well an enclosure can attenuate or block electromagnetic waves, essentially shielding sensitive electronics from the harmful effects of electromagnetic interference (EMI).

When measuring in a reverberation chamber, the SE can be defined as the ratio of the average power density of the incident electromagnetic waves to the average power density of the transmitted waves inside the enclosure. In metallic enclosures, the incident electromagnetic power density solely penetrates through apertures. The walls of the enclosure, and the enclosed objects contribute to attenuation through reflection and partial absorption, depending on the enclosures and object's conductivity and the wave frequency.

The average transmission cross section (ATCS) quantifies the ability of an aperture to transmit incident electromagnetic waves into the enclosure and the average absorption cross sections (AACS) measure the ability of the enclosure walls and the contents to absorb incident electromagnetic waves. For an electrically large enclosure, which can be considered reverberant, accurately predicting the SE of an enclosure becomes complex when its interior contents vary.

Our proposed method is an advancement to the Power Balance technique and uses the ATCS of the aperture and the AACS of the walls to predict SE with diverse contents. The incident electromagnetic wave interacts with the apertures, walls, and contents within the cavity, leading to transmission, reflection, and absorption. By incorporating the measured or calculated ATCS and AACS of each element, we can mathematically model these interactions and predict the overall SE for a specific content configuration with known AACS. By accounting for the specific characteristics of both the enclosure and its contents, the predictions enable the SE of the enclosure with the specific contents to be evaluated rather than the SE of an empty enclosure as with other techniques.

The method can be readily adapted to various enclosure designs and content configurations, making it a powerful tool for diverse applications even for the enclosure with electrically small apertures. By incorporating the concepts of transmission and absorption cross sections, our proposed method paves the way for more accurate and versatile SE predictions and can revolutionize the design of effective EMI shielding solutions, ensuring the reliable operation of electronic systems in an increasingly electromagnetically cluttered world.

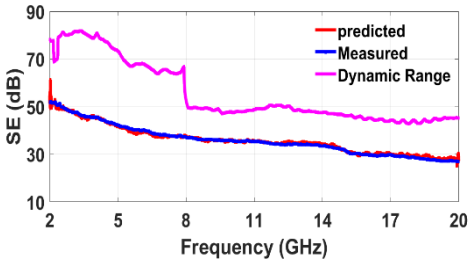

Figure 1. The comparison of predicted and measured values of the SE shown in Fig. 2

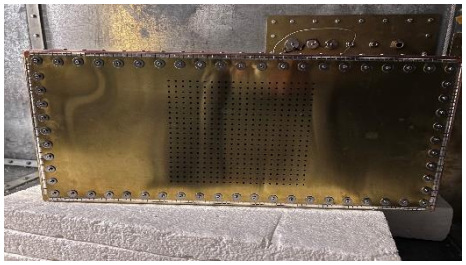

Figure 2. The enclosure and the aperture comprising an array of circular holes – the enclosure's dimension is 300×500×600 (mm)

This project has received funding from the European Union's EU Framework Programme for Research and Innovation Europe Horizon (Grant Agreement No 101072881, for Doctoral Researcher Positions 1-4, 6-8 and 10-12) and UKRI (UK Research and Innovation, for Doctoral Researcher Positions DR5 and DR9).

Abdul Jabbar(abdul.jabbar@glasgow.ac.uk)

The 2024 URSI UK Symposium (URSI UK Symposium 2024)

Abstract

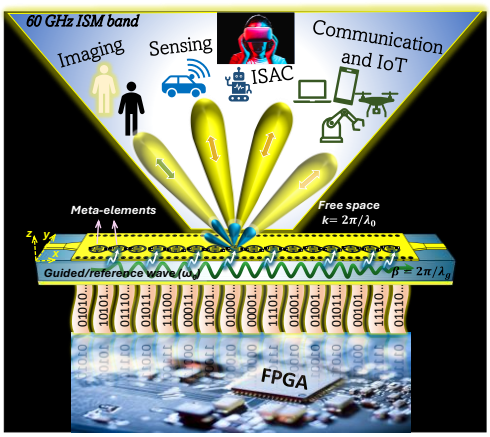

The next-generation (beyond 5G and 6G) wireless technologies are envisioned to adapt to dynamic environments through intelligent and software-reconfigurable paradigms to maintain the quality of service and seamless connectivity. In recent years, dynamically tunable coded metasurfaces have been explored widely whose operational status can be electronically reconfigured, such as reconfigurable intelligent surfaces (RIS) and coded reflect/transmit metasurface arrays. However, these surfaces work on the principle of "reflection" rather than "radiation". Moreover, these passive surfaces need to be fed through an external source antenna and hence the whole network becomes quite bulky.

On the contrary, ***Dynamic Metasurface Antenna (DMA)*** is an emerging antenna technology under the paradigm of "radiative metasurfaces". A DMA offers agile and reconfigurable radiation pattern diversity and adaptability from a simplified, low-cost, and low-profile hardware platform with an active in-plane excitation feed. It avoids the use of complex and lossy feed networks as well as power-hungry and bulky phase shifters, thereby offering versatile and low-cost electronic beamforming capabilities. Recently some initial investigations on DMA prototypes have been reported at lower microwave bands, however, there is no practical DMA hardware prototype available at higher frequency bands, such as around 60 GHz and sub-THz.

We have developed a DMA array hardware prototype at 60 GHz industrial, scientific, and medical (ISM) band that is fully programmable and offers dynamic electronic beam-steering controlled through an in-house designed high-speed FPGA. The constituent radiating elements of a DMA are magnetic dipoles which are fed through a low-loss planar substrate integrated waveguide aperture. The meta-elements are meticulously designed around 60 GHz with fully addressable 1-bit control using integrated PIN didoes. A 4-layer PCB is designed with a compact size, and extensive optimization has provided -10 dB impedance bandwidth covering 59 GHz to 62 GHz, with beamforming gain of above 10 dBi at different coding sequences, high radiation efficiency, and below -10 dB side lobe level over a wide range of angular span. Our DMA prototype offers synthesizing various types of beam patterns such as narrow beams, wider beams as well as multiple beams from a single antenna aperture, based on selective coding sequence. performance in real-time with an overall beam-steering delay (agility) of about 5 ns.

With a notion of adaptability to the dynamic reconfigurability of EM environment in 6G technologies, we designed the DMA prototype in a flexible and programmable manner to work with various beamforming and signal processing algorithms. The versatility of our 60 GHz DMA prototype provides an off-the-shelf solution to explore and test a diverse range of next-generation mmWave applications encompassing 6G holographic communication, sensing and imaging, cognitive radars, high-resolution mmWave sensing and localization, contact-less smart healthcare, 60 GHz mmWave smart wireless factories, as well as integrated sensing and communication (ISAC) avenues.

URSI UK Abstract Submission

Name: Natalie Reeves
Due Date: 22/01/2024

Understanding the sensitivity of the thermosphere and ionosphere to solar and geomagnetic conditions is critical for space weather predictions. This study aims to use Global Sensitivity Analysis (GSA) techniques to evaluate how K_p and F10.7 daily averages can influence Thermosphere Ionosphere Electrodynamics General Circulation Model (TIE-GCM) output (e.g., electron density, total electron content and solar wind parameters). Each model input was varied individually, and the induced variations are visually and quantitatively compared to model predictions. This analysis looks at the robustness of simulated results with the purpose of generating better ensembles for the Advanced Ensemble Electron Density (Ne) Assimilative System (AENeAS) forecasting model. Since AENeAS uses TIE-GCM as a background model and to propagate the model densities forward in time.

Multi-band UHF RFID Reader Antenna Design

Ibrahim Gharbia[1], Atta Ullah[1], Abubakar Salisu[1], and Raed A Abd-Alhameed[1]

[1]Biomedical and Electronics Engineering, Faculty of Engineering and Informatics,
University of Bradford, Bradford, BD7 1DP, UK
i.o.i.gharbia@bradford.ac.uk[1]

Globally the UHF was divided into regions, such as 868MHz in Europe or 902-928 MHz in the USA and Australia, and lastly 2.4-2.4835GHz across the world. Circularly polarised patch antenna that was developed specifically for use with RFID readers. In multi-band antenna design, some proposed designs add some electronic devices to meet the frequencies needed and to cancel other frequencies. On the other hand, other designs meet the frequencies needed without the need to add any electronic components. In this study, the major emphasis is to design an antenna that has wideband CP without adding any electronic components [1-3]. This design can operate on all available UHF frequencies for RFID usage applications. The following acceptable results that this antenna achieved, for S_{11} are as follows: S_{11} = -11.8 dB when the frequency is set to 0.868 GHz, S_{11} = -11.08 dB when the frequency is set to 0.902 GHz, S_{11} = -10.47 dB when the frequency is set to 0.928 GHz, S_{11} = -16.83 dB when the frequency is set to 2.4 GHz, and S_{11} = -13.25 dB when the frequency is set to 2.4835 GHz. We introduce a multiband circular polarisation antenna with a question mark-shaped antenna that is partly shielded by the ground as shown in Figure 1. By adding a rectangular stub and substrate two other rectangular to the ground including the addition of a semi-circular to the upper terminal of the feeding line the proposed antenna significantly improved. The simulated results are quite promising compared to our previous work in [1]. The antenna is mounted on FR4 substrates with a dielectric constant of 4.3 relative permittivity and 0.025 tangent loss. The dimensions of the whole antenna structure are 250 x 250 x 1.6 mm^3. A 50Ω microstrip feed line connected to the proposed antenna to form a wideband planar monopole antenna; in addition, a stub has been attached to the ground plane to improve the axial ratio bandwidth (ARBW). Further enhancement in the ARBW has been acquired after engraving a slit on the patch of the proposed antenna in addition to attaching a semicircular stub with a radius $r = 15$ at the top of the feed line.

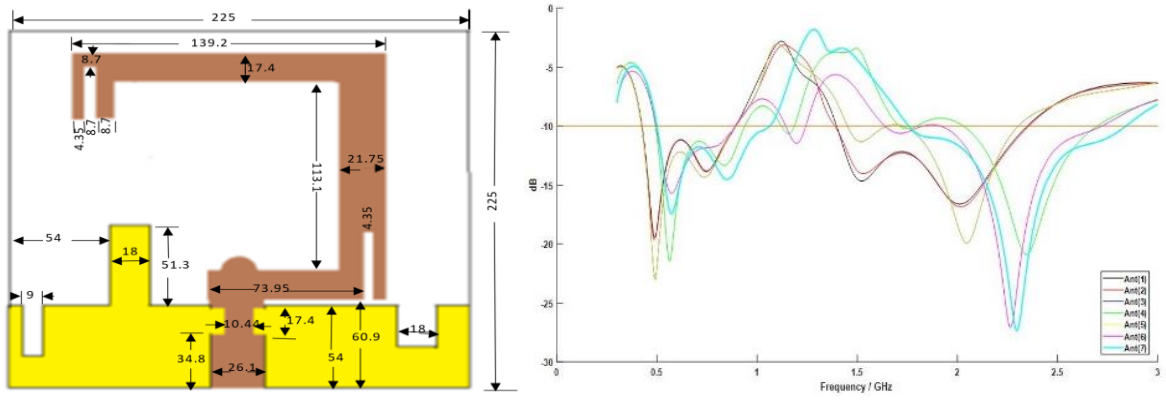

(a) (b)

Figure 1: Proposed antenna geometry (a), and the spectrum reflection of multi-bands (b).

References:

1. F. M. Alnahwi, I. Ghariba and et.al., A Compact Wideband Circularly Polarized Planar Monopole Antenna With Axial Ratio Bandwidth entirely encompassing the antenna bandwidth. IEEE Access, August, 2022.
2. Sayan Sarkar BG. A Dual frequency Circularly Polarized UHV-RFID/ WLAN Circular Patch antenna for RFID Readers. In IEEE; 2019; Pisa, Italy, IEEE. p. 100-120.
3. Parthiban P. An Ultra-Rugged UHF RFID Reader Antenna. IEEE. 2020 February ; 62(1): 84-92.

Near-Field Localization with an Exact Propagation Model in the Presence of Mutual Coupling

Zhoreh Ebadi, Queen's University Belfast, UK

Abstract—Localizing near-field sources considering practical arrays is important in wireless communications. Array-based apertures exhibit mutual coupling between the array elements, which can significantly degrade the performance of the localization method. In this paper, we propose two methods to localize near-field sources by direction of arrival (DOA) and range estimations in the presence of mutual coupling. The first method utilizes a two-dimensional search to estimate DOA and the range of the source. Therefore, it suffers from a high computational load. The second method reduces the two-dimensional search to one-dimensional, thus decreasing the computational complexity while offering similar DOA and range estimation performance. Besides, our second method reduces computational time by over 50% compared to the multiple signal classification (MUSIC) algorithm.

Low Noise Amplifier Based Heterodyne Highly Integrated Receivers for Millimetre and Sub-millimetre Wavelength Radio Astronomy

William McGenn[1*], Hui Wang[2], Elle Franks[1], Brian Ellison[1], Gary A. Fuller[1], Danielle George[1], Peter G. Huggard[2]

[1]Advanced Radio Instrumentation Group, University of Manchester, Manchester, M13 9PL, UK.
[2]Millimetre Wave Technology Group, STFC Rutherford Appleton Laboratory, Didcot, Ox11 0QX, UK.
[*]email: william.mcgenn@manchester.ac.uk

Developments in sub-100 nm gate length Indium Phosphide (InP) Pseudomorphic High Electron Mobility Transistor (pHEMT) technology has pushed the boundaries of Low Noise Amplifiers (LNAs) [1, 2], allowing the design and fabrication of LNA based heterodyne receivers for the millimetre and sub-millimetre wavelength bands of radio telescopes. Typically, radio telescope receivers are constructed from individual components that are packaged in separate metal blocks, as is the case for the recent state-of-the-art ALMA Band 2 receivers [3]. There are several benefits of this approach, but it does not result in the most space efficient receiver format, each of the sub-components needs to contain all of the associated circuity within its block and to have a predefined precision mechanical interface. Whilst this discrete approach is viable at lower frequencies or for a single receiver 'pixel', as operating frequencies increase and complex multi-pixel receiver topologies are required for enhanced observation speed, a more space efficient and integrated approach to LNA and overall receiver design is needed.

The Millimetre Wave Technology Group and the Technology Department at the STFC Rutherford Appleton Laboratory and the University of Manchester Advanced Radio Instrumentation Group have recently completed the sixteen-pixel, W-band (70-116 GHz) Cryogenic Array Receiver for Users of the Sardinia Observatory (CARUSO) receiver. The development of this receiver pushed the designs of the individual components to the physical limits of what is achievable to ensure that the components of the receiver chain in each pixel will fit within the footprint of the closely packed feedhorns, while still allowing access for DC bias, local oscillator and intermediate frequency signal ports. Moreover, the complete assembly needed to be contained within a vacuum shroud and attached to a cryogenic cooler to support operation at temperatures ≤ 20K.

With this in mind, we are now investigating methods of realizing a future fully integrated millimeter-wave receiver as part of the ESO funded TASER and EU funded RADIOBLOCKS projects. Here we will present the first steps towards this goal, of a study on the integration of the LNA and Subharmonic Image Rejection Mixer (SHIRM) [4] components, and discuss potential strategies for further miniaturization and integration, as well as the impact that these design choices will have on the fabrication and characterization process.

Acknowledgements

The authors would like to acknowledge the support of Carlos De Breuck, Tony Mroczkowski and Gie Han Tan of the European Southern Observatory (ESO) as part of the ESO funded *TASER: Towards ALMA System on Chip European Receivers* project. The RADIOBLOCKS project has received funding from the European Union's Horizon Europe research and innovation programme under grant agreement No 101093934

References

[1] D. White, et al. *"125 - 211 GHz low noise MMIC amplifier design for radio astronomy"*. Exp Astron 48, 137–143 (2019). https://doi.org/10.1007/s10686-019-09641-z
[2] D. Cuadrado-Calle et al., *"Broadband MMIC LNAs for ALMA Band 2+3 With Noise Temperature Below 28 K,"* IEEE Trans. on Microwave Theory and Techniques 65, pp. 1589-1597, 2017, doi: 10.1109/TMTT.2016.2639018.
[3] P. Yagoubov, et. al. *"Wideband 67-116 GHz receiver development for ALMA Band 2."* Astronomy & Astrophysics, 634: A46, 2020. doi: 10.1051/0004-6361/201936777
[4] H. Wang, *et al., "Pre-prototype ALMA Band 2+3 Down-Converter & Local Oscillator System"*, proceedings of the 28th International Symposium on Space Terahertz Technology, Cologne, Germany, March 13-15, 2017.

Towards Minimal Negative Static Electric Susceptibility: Crystal Engineering in Active Metamaterials

Rahul Dutta,[*] Flynn Castles, and Yang Hao

School of Electronic Engineering and Computer Science, Queen Mary University of London, Mile End Road, London E1 4NS, United Kingdom

[*]r.dutta@qmul.ac.uk

The discovery and development of materials with new or enhanced properties is an important driver of technological advance. In the area of electrostatics and low-frequency electromagnetics, a key material property is static electric susceptibility $\chi^{(0)}$ [or, equivalently, static relative permittivity $\varepsilon^{(0)}$, related via $\varepsilon^{(0)} = \chi^{(0)} + 1$]. Although well-established textbook arguments suggest that static electric susceptibility $\chi^{(0)}$ must be positive in "all bodies" [1], it has been pointed out that materials that are not in thermodynamic equilibrium are not necessarily subject to this restriction [2-5]. The possibility of $\chi^{(0)} < 0$ in metastable systems with inverted populations has been discussed tentatively by Sanders [2,3], and Chiao *et al*. predicted unequivocally a $\chi^{(0)} < 0$ state in such systems [4,5]. More recently, it was proposed that $\chi^{(0)} < 0$ may also be achieved in completely different systems, e.g., active metamaterials [6]. In addition, a preliminary experimental affirmation in support of the general concept was also reported obtaining magnitudes of negative static electric susceptibility much greater than the systems of Sanders and of Chiao et al. [6]. This led to the understanding that alongside the existence of $\chi^{(0)} < 0$, relatively large magnitudes of the property can also be obtained which are expected to be crucial in the realization of devices capable of the novel phenomenon of levitation using static electric fields (analogous to the well-known phenomenon of diamagnetic levitation in static magnetic fields). With the ongoing practical development of condensed (meta)materials owning relatively large magnitudes of negative static electric susceptibility, it appeared timely to determine rigorously how negative one can expect the negative static electric susceptibility to be made in non-equilibrium condensed materials. In [6], it was claimed — without full theoretical or experimental justification — that negative static electric susceptibility is possible for all values in the interval $\{\chi^{(0)}: -1 < \chi^{(0)} < 0\}$; the theoretical basis on which this claim was made is presented in [7]. We have found that $\chi^{(0)} < 0$ values are possible for nonequilibrium cubic crystals, and that the lower bound for certain crystal structures (bcc and fcc) are exactly -1. We also found that the lower bound is structure-dependant, differing for sc than for bcc and fcc. Determining the lower bound for a specific crystal structure is generally nontrivial and likely requires methods akin to those in [7]. While assumptions in [7] may introduce inaccuracies regarding real systems, our findings indicate a preference for bcc or fcc structure over sc structure when aiming to create isotropic material with minimum $\chi^{(0)}$ from identical entities.

References

[1] L. D. Landau, E. M. Lifshitz, and L. P. Pitaevskii, Electrodynamics of Continuous Media (Course of Theoretical Physics, Vol. 8), 2nd ed. (Butterworth-Heinemann, Oxford, UK, 1984).

[2] T. M. Sanders, Jr., The sign of the static susceptibility, Bull. Am. Phys. Soc. 31, 868 (1986).

[3] T. M. Sanders, Jr., On the sign of the static susceptibility, Am. J. Phys. 56, 448 (1988).

[4] R. Y. Chiao and J. Boyce, Superluminality, parelectricity, and earnshaw's theorem in media with inverted populations, Phys. Rev. Lett. 73, 3383 (1994).

[5] R. Y. Chiao, E. Bolda, J. Bowie, J. Boyce, J. C. Garrison, and M. W. Mitchell, Superluminality and parelectric effects in rubidium vapour and ammonia gas, Quantum Semiclass. Opt. 7, 279 (1995).

[6] F. Castles, J. A. J. Fells, D. Isakov, S. M. Morris, A. A. R. Watt, and P. S. Grant, Active metamaterials with negative static electric susceptibility, Adv. Mater. 32, 1904863 (2020).

[7] R. Dutta, P. D. Wurzner, F. Castles, Lower negative bounds on the static electric susceptibility of nonequilibrium cubic crystals, Phys. Rev. B 109, 045109 (2024).

A RF Propagation Modelling Methodology for Determining the Level and Nature of Scattering from Measurements

Sanchita Kayal, Geoffrey Hilton, and Mark Beach*

Communication Systems and Networks Group, University of Bristol, BS8 1UB, UK

**s.kayal@bristol.ac.uk*

Wireless network evolution, spanning macro to micro elements, defies a universal modelling due to diverse channel responses. Tailoring accurate channel models for a dedicated applications like body area networks and urban communication [1-2] is paramount. Existing literature drawing from measurement and simulation [3-4] meets challenges, but a gradual surge of paradigm shift in millimeter-wave bands, emphasizes surface attributes (texture, granularity) over traditional properties [5]. While traditional tools suffice below 6 GHz, the ascent in frequency requires a profound understanding of scattering. Hence, the challenge involves comprehending the interplay between objects and waves across various angles, even in simulations. This pursuit necessitates resilience in scientific efforts to unravel wireless network complexities.

This study proposes a robust channel modelling approach using sparse Angle of Arrival (AoA) and Angle of Departure (AoD). It establishes a foundational framework by gradually introducing objects, irrespective of applications. Centred on metal objects in non-line-of-sight (nLoS) links, it explores their impact on signal transmission. The investigation, considering co-polar and cross-polar orientations, enhances understanding of electromagnetic polarization's role in signal quality and strength. Prior to taking on more intricate structures, it is imperative to master the correct procedures, the simplest case as a benchmark. Therefore, a sample metal plate is used to differentiate the reflection from the (baulk) material and the diffraction from its edges, thus be able to determine the scattering properties regardless of sample size considering the fact that a larger sample would tend to have a higher effective reflecting gain. Although, this measurements apply to any frequency, the data in this work will be presented at 3.5GHz.

The analysis with the metal plate establishes foundational benchmarks in terms of gain, beamwidth, and sidelobes for comparisons with Radar Cross Section (RCS) of more complex structures, including those with corrugation, varied material properties, or advanced technologies like Reconfigurable Intelligent Surfaces (RIS). Controlled environment allows focused analysis of reflection, scattering, and diffraction phenomena associated with the metal object. Additionally, a specifically chosen configuration [6] prioritizes signals influenced by nLoS components over direct ones. The use of a 90-degree transmit-receive offset is crucial, establishing a direct link between measured beamwidth and twice that of the reflected signal at a fixed angle of illumination. This unique setup provides a fresh perspective on data, closely tied to signal arrival and departure angles, enhancing insights with relevance to literature.

References

[1] S. Ambroziak, L. Correia, R. Katulski, M. Mackowiak, C. Oliveira, J. Sadowski, et. al., An Off-Body Channel Model for Body Area Networks in Indoor Environments. IEEE Trans. Antennas Propag.,vol. 64, 2016.

[2] M. R. Arias, B. Manderson, Clustering Approach for Geometrically Based Channel Model in Urban Environments. IEEE Antennas and Wireless Propagation Letters, vol. 5, pp. 290-293, 2006.

[3] X. Zhou, S. Wang, D. Zhang, B. Wang, Sub-6GHz Channel Measurements and Modeling for City Underground Power Pipe Gallery. IEEE 5th International Conference on Electronics Technology (ICET), pp. 848-852, Chengdu, China, 2022.

[4] J. H. Lee, J. S. Choi, J. Y. Lee, S. C. Kim, 28 GHz Millimeter Wave Channel Models in Urban Microcell Environment Using Three Dimensional Ray Tracing. IEEE Antennas and Wireless Propagation Letters, vol. 17, no. 3, pp. 426-429, March 2018.

[5] C. Anioke, C. Nnamani, C. Ani, Investigating Indoor Scattering at mmWave Frequencies. International Journal of Scientific and Technology Research, vol. 9. pp. 554-560, 2020.

[6] A. K. B. M. ISA,Practical RF Material Characterisation Methodology for K-band and Millimetre wave Frequency. University of Bristol, PhD Dissertation, January 2020.

Low Noise Amplifier Characterisation Automation with the CryoMe Software Package

E. Franks, W. McGenn, C. Jarufe, L. Jiang, G.A. Fuller, D. George

Advanced Radio Instrumentation Group, University of Manchester, Manchester, UK

The sensitivity of radio receivers can be optimised by using a high gain Low Noise Amplifier (LNA) as close to the front-end as possible in order to reduce the noise contributions from the following stages [1]. Because of this, radio telescopes operating in the microwave, millimetre, and increasingly the sub-millimetre wavelengths generally make use of cryogenically cooled High Electron Mobility Transistor (HEMT) based LNAs as their initial receiver gain blocks.

LNA fabrication, assembly, and characterisation make sure performance specifications are met in the radio telescope production process. Part of the characterisation process is the measurement of LNA gain and noise performance over operational bandwidth, at the intended operating temperature. For each LNA, processing differences will cause different bias conditions (i.e. different drain voltages and currents) to give different performance, so ideally multiple bias points are tested as a part of instrument optimisation. Large-scale telescope arrays, focal plane arrays, and phased array feeds are increasingly common in radio astronomy, and all require many more LNAs than have been typical for previous projects. With the consequent demand increase, testing will become a very time-consuming part of a project.

To speed up LNA testing on the recently completed CARUSO receiver project, which required over one hundred LNAs in the 67-116 GHz frequency range, we have built a three-channel cryostat and an automated measurement system. To automate the process of LNA characterization/measurement, we have developed a new software package named *CryoMe.* Features include automated cryogenic Y-Factor measurements, automated sweeps of bias conditions, a safe adaptive drain current seeking algorithm, and output data analysis. The test equipment is controlled to bias an LNA, retain desired ambient/load temperatures, and, over a requested frequency bandwidth, perform power measurements. A computer-controlled waveguide switch allows *CryoMe* to automate the measurement of each chain in a single cooling cycle, allowing three LNAs to be characterised in full overnight. Output data is analysed giving several characterisation metrics such as the calibrated gain and noise measurements of an LNA under test. In comparison to manual measurement, this is a far quicker, comprehensive, and reliable process.

A major *CryoMe* output is heat maps of gain and noise performance plotted against the set bias conditions, which allows very easy identification of optimum bias points. CryoMe can be used on either single independent LNAs, or it can be used to tune amplifiers in a receiver in situ. Results can be easily reprocessed with different calibration data, and analysis can be performed on sub-bandwidths upon request. In comparison to a manual measurement system, *CryoMe* has shown it improves the speed of characterisation significantly.

An overview of the cryostat setup, and discussion of the capabilities, and features of CryoMe, as well as its benefits (i.e. speed, utility, and throughput) will be presented. Sample outputs will be shown. I will also give examples of some of the use cases of this software package and testing approach.

[1] I.D. Robertson and S. Lucyszyn, *RFIC and MMIC Design and Technology*, IET, Stevenage, 2001.

Extending Quasilinear Theory for Particles Near 90°

Authors:
Samuel Boardman*[(1)], Oliver Allanson[(1)], Adnane Osmane[(2)] and Sean Elvidge[(1)]

Groups:

1. **Space Environment and Radio Engineering (SERENE); Electronic, Electrical and Systems Engineering; School of Engineering; University of Birmingham; Birmingham; UK; email: sxb1796@student.bham.ac.uk**
2. **Department of Physics; University of Helsinki; Helsinki; Finland**

Energetic electron populations that are present in the Earth's outer radiation belt are an outstanding natural environment allowing us to discover the nature of how the dynamics of relativistic charged particles evolve, how they are lost, and how they are accelerated.

These radiation belt electrons are trapped when pitch angles are outside the loss cone. Losses and acceleration are well accounted for when considering wave-particle interactions where particles have pitch angles in central values. However, current models rely on a quasilinear theory that does not explain the observable loss rates of particles with pitch angles near 90 degrees. One possible solution to this 90-degree problem is resonance broadening, wherein wave-particle interactions can occur at a range of wavelengths near to the resonant value rather than only for perfect resonance.

Here we will highlight a derivation of diffusion coefficients under the weak turbulence approximation before suggesting and analysing links with a potential nonlinear extension to quasilinear theory.

Enhancing Patient Monitoring Systems Through Differential Power Gains and Time Delay Series emanating from RFID Sensors.

Ebenezer Adjei[1], Prince O. Siaw[1], Ahmad Aldelemy[1], Raed A. Abd-Alhameed[1] Mohamed Lashab[2]
[1]Faculty of Engineering and Digital Technology, University of Bradford, United Kingdom
[2]Department of Electronics, University of Oum El Bouagui, Oum El Bouagui, Algeria

e.adjei@bradford.ac.uk [1] p.o.siaw@bradford.ac.uk[1], a.a.aldelemy@bradford.ac.uk
[1]r.a.a.abd@bradford.ac.uk[1], Lashabmoh@gmail.com[2],

The growing population of elderly individuals in society has led to a significant advancement in the integration of IoT and wireless communication technologies [1]. This integration aims to enhance the patient monitoring system in healthcare services. The primary objective of this study was to determine the location of patients within a smart room setting by analysing the varying levels of received power from wireless sensors, specifically RFID technology. The proposed system is designed using four sophisticated intelligent models to accurately measure power for location and position detection. The neural network in MATLAB acquired knowledge about the measured power transfer to verify the accuracy of its predictions.

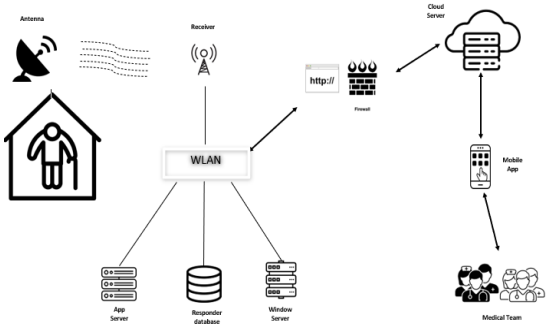

Figure 1. An image depicting the system architecture of the proposed smart room system for remote monitoring.

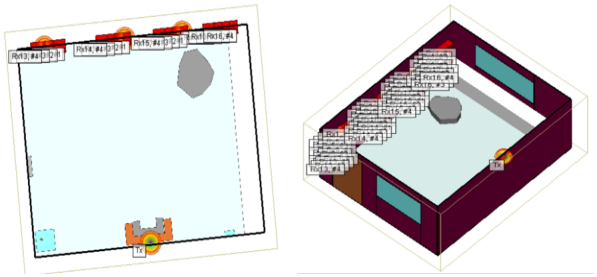

Figure 2. An image of the designed smart smart room using the Wireless Insite software.

The Wireless Insite software was used to model a smart room with all material properties in the room included in the design to mimic a real-life standard room. A human model was designed with three different orientations (standing, sitting, and lying down). Each orientation was introduced to the empty smart room and simulation was run five times. This was repeated for the remaining orientations and the data obtained was fed to the neural network in MATLAB to train the system for real time prediction in future.

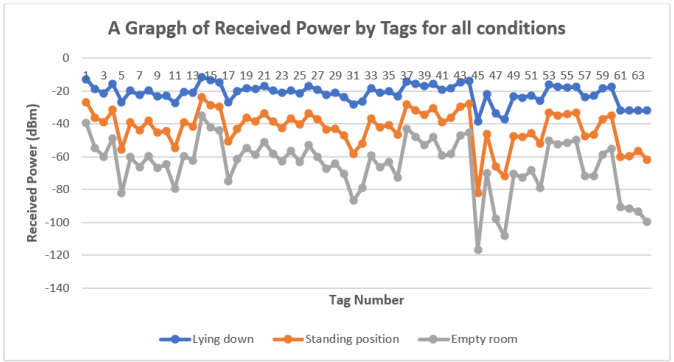

Figure 1. A graph of received powers emanating from the RFID. tags during the simulations.

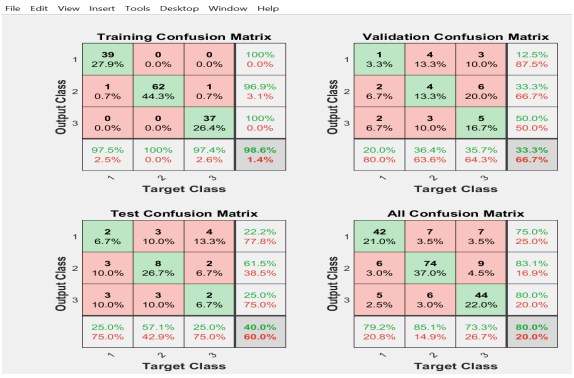

Figure 2. image of the Neural Network indicating the accuracy of its predictions per the orientation of the patient.

The simulation results indicate that the proposed smart room system can replace the existing techniques of remote patient monitoring with increased reliability.

References

1. MICHEL, J.-P., LEONARDI, M., MARTIN, M. & PRINA, M. 2021. WHO's report for the decade of healthy ageing 2021–30 sets the stage for globally comparable data on healthy ageing. *The Lancet Healthy Longevity,* 2**,** e121-e122.
2. BIANCO, G. M., OCCHIUZZI, C., PANUNZIO, N. & MARROCCO, G. 2021. A survey on radio frequency identification as a scalable technology to face pandemics. *IEEE Journal of Radio Frequency Identification,* 6**,** 77-96.

URSI UK Symposium 2024, NPL, Teddington, UK, 21 Feb 2024

Design and Preliminary Indoor Assessment of a Long-Range sub-THz VNA-Based Channel Sounderbetween 500 GHz and 750 GHz

Lawrence Carslake[(1)], James Skinner [(1)], and Tian Hong Loh[(1)]
(1) Electromagnetic & Electrochemical Technologies, National Physical Laboratory, Teddington, United Kingdom; e-mail lawrence.carslake@npl.co.uk, james.skinner@npl.co.uk, tian.loh@npl.co.uk

Traceable sub-Terahertz (sub-THz) propagation channel characterization is necessary for the successful development of new applications of these sub-Thz frequencies. Through published sub-THz channel propagation models, new devices can be designed and verified through simulations before prototyping decreasing the development time of new communications applications. This paper presents the design and initial testing of a novel long-range vector network analyzer based sub-THz channel sounding system with the capability of antenna separations up to 600m. Enabling the measurement of long-range 500 – 750 GHz channels and subsequent development of channel propagation models.

The designed system addresses the technical difficulties encountered with co-axial cable losses that have restricted the antenna separations of current sub-Thz channel sounding systems. The overall propagation path of these previous sub-THz channel sounding systems between transmitter and receiver is limited to 10 m for [1], 0.23 m for [2], and 3.85 m for [3]. The use of a phase-compensated optical fiber system in this channel sounder, established in [4], allows for significantly increased measurement distances while maintaining system calibration and has been evaluated with connection lengths up to 600 m. A full link budget assessment has been performed with the 600 m optical and co-axial connections, to verify the measurement dynamic range and the operation of the remote frequency extender unit.

The operation of the phase-compensated optical fiber system has been further verified at 500- 750 GHz, through the comparison measurements of the system with the optical fiber included and additionally removed. Operation in both these cases is shown to be closely matching, demonstrating the equivalence of measurements which have been extended by the optical fiber system. The system has then been used to perform preliminary indoor channel sounding, with an antenna separation of up to 4.48m, connected by 600m of optical fiber and co-axial cables. The peaks in the measured path magnitude located at 4.68 ns and 15.02 ns, in the two tested separations show correlation with the calculated line-of-sight path delays, 4.64 ns and 14.9 ns for 1.39 m and 4.48 m separations respectively.

The project (21NRM03 MEWS) has received funding from the European Partnership on Metrology, co-financed from the European Union's Horizon Europe Research and Innovation Programme and by the Participating States. Funded by the European Union. Views and opinions expressed are however those of the author(s) only and do not necessarily reflect those of the European Union or EURAMET. Neither the European Union nor the granting authority can be held responsible for them.

1. Y. Lyu, P. Kyösti and W. Fan, "Sub-THz VNA-based Channel Sounder Structure and Channel Measurements at 100 and 300 GHz", 2021 IEEE 32nd Annual International Symposium on Personal, Indoor and Mobile Radio Communications (PIMRC 2021), Helsinki, Finland, 2021, pp. 1-5

2. D. Serghiou et al., "Ultra-Wideband Terahertz Channel Propagation Measurements from 500 to 750 GHz" 2020 International Conference on UK-China Emerging Technologies (UCET 2020), Glasgow, UK, 2020, pp. 1-4

3. M. Schmieder, W. Keusgen, M. Peter, et al., "THz Channel Sounding: Design and Validation of a High Performance Channel Sounder at 300 GHz," 2020 IEEE Wireless Communications and Networking Conference Workshops (WCNCW 2020), Seoul, Korea, 2020, pp. 1–6.

4. Y. Lyu, A. W. Mbugua, K. Olesen, P. Kyösti and W. Fan, "Design and Validation of the Phase-Compensated Long-Range Sub-THz VNA-Based Channel Sounder", IEEE Antennas and Wireless Propagation Letters, Vol. 20, No. 12, pp. 2461-2465, Dec. 2021

Reconfigurable Dual Band Antenna with Ultra-wide Bandwidth Operating at Sub 6GHz and Millimeter Wave Bands For 5G Mobile Applications.

Abubakar Salisu[14*], Atta Ullah[1], Umar Musa[2], Mobayode O. Akinsolu [3], Ibrahim Gharbia[1] , Ahmad Aldelemy[1], A. S. Hussaini [1,5], and Raed A Abd-Alhameed[1].
[1]Department of Electronics and Biomedical Engineering, University of Bradford, United Kingdom
[2]Department of Electrical Engineering, Bayero University Kano, Nigeria
[3]Faculty of Arts, Science and Technology, Wrexham Glyndwr University, LL11 2AW Wrexham, U.K.
[4]Department of Electrical and Electronics Engineering, MAU Yola, Nigeria
[5]School of Engineering, American University of Nigeria, Yola
[*]Corresponding email: a.salisu@bradford.ac.uk

Recently, Researchers have been interested in multi-band reconfigurable antennas with an improved bandwidth because of the potential for breakthroughs in the integration and reconfiguration of the sub-6 GHz and mm-wave bands. Small, frequency-configurable antennas are needed for future 5G technology to use all available wireless bands (such as the sub-6 GHz and mm-wave bands). The fastest 5G services need roughly 100 MHz of bandwidth in the 5G mid-band (3.5 GHz) and 1 GHz bandwidth in the mm-wave spectrum to accommodate enormous volumes of traffic at high data rates (28 GHz). In this study, a small, dual-band, frequency-configurable antenna with a larger bandwidth for use in upcoming 5G mobile devices is presented. The suggested antenna uses a radio frequency (RF) PIN diode (SMP 1321-079LF) switch to toggle between two operating modes, providing a maximum frequency range of 3.39-3.66 GHz (ON state) and 27.40-28.60 GHz (OFF state) for usage in 5G networks, by combining a meandering radiating patch with a truncated ground structure; a size reduction and bandwidth improvement were accomplished.

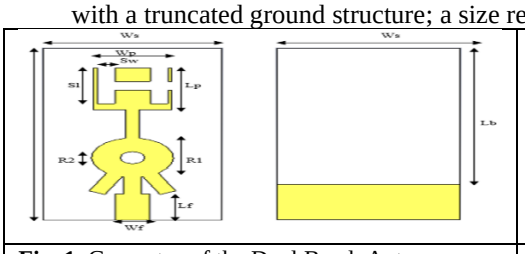

Fig. 1. Geometry of the Dual Band Antenna

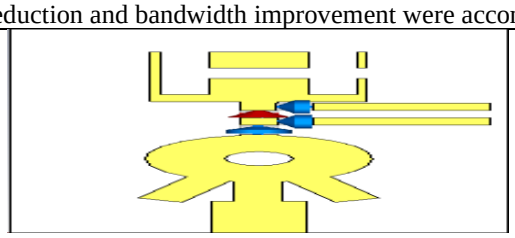

Fig2. Reconfigurable Antenna with PINDiodes

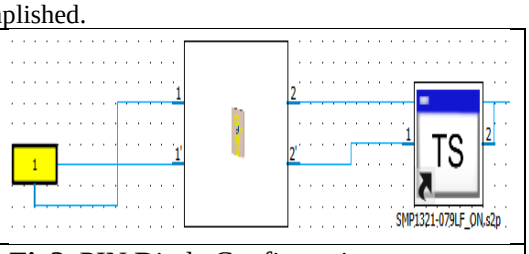

Fig3. PIN Diode Configuration

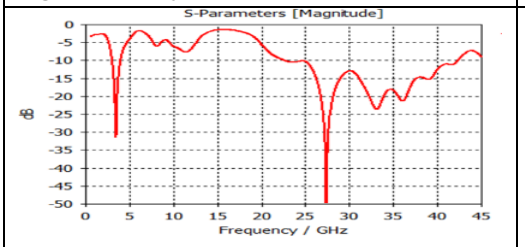

Fig4. S11 Results Before Configuration

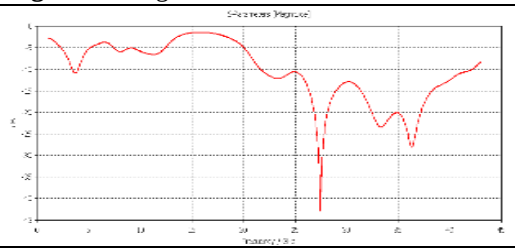

Fig5. Results After Configuration

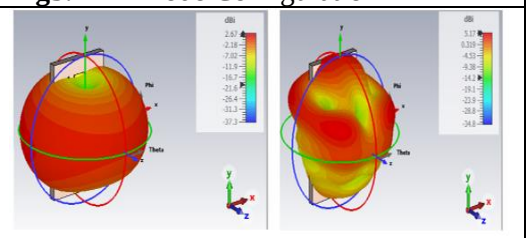

Fig5. Gain of the Proposed Antenna

The proposed reconfigurable dual-band antenna switching between millimeter wave and sub-6 GHz bands is a necktie round shape patch design connected with a meandered radiating patch element at the top front with an H slot shape and a partial or truncated ground plane at the back to enhance the antenna's functionality and performance. The dual band antenna is designed using CST microwave studio on a substrate Rogers 3003 with a dimension of 27.8 mm x 14mm and thickness of 1.52 mm with a dielectric constant of 2.2 and a loss tangent of 0.0009 respectively. The PIN diode (SMP 1321-079LF) is placed between the two parts to resonate the antenna at 3.5 and 28 GHz by altering the switching state. During the ON state of the PIN diode, the antenna operates at both 3.5 GHz and 28 GHz; whereas, in the OFF state, it operates in the mm-wave band at 28 GHz, thereby eliminating the 3.5 GHz band. The proposed antenna has an ultra-wide bandwidth of 19.65 GHz covering almost all the milli meter wave bands of 23 GHz, 28 GHz, and 38 GHz (from 22.65 – 42.30 GHz) while the sub-6 GHz band has a bandwidth of 962 MHz (3.02 – 3.99 GHz) respectively. The return loss of the antenna is -31.33 dB and -49.72 dB at 3.5 GHz and 28 GHz respectively. However, this antenna is compact and combines two different frequency bands with a larger bandwidth, and the frequency ratio between the millimeter wave band to the sub-6 GHz band is 8.

[1] M. Ikram, E. A. Abbas, N. Nguyen-Trong, K. H. Sayidmarie, and A. Abbosh, ‘‘Integrated frequency-reconfigurable slot antenna and connected slot antenna array for 4G and 5G mobile handsets,’’ IEEE Trans. Antennas Propag., vol. 67, no. 12, pp. 7225–7233, Dec. 2019.

[2] M. Zada, I. A. Shah and H. Yoo, "Integration of Sub-6-GHz and mm-Wave Bands With a Large Frequency Ratio for Future 5G MIMO Applications," in IEEE Access, vol. 9, pp. 11241-11251, 2021, doi: 10.1109/ACCESS.2021.3051066.

[3] W. Hong, K.-H. Baek, and S. Ko, ‘‘Millimeter-wave 5G antennas for smartphones: Overview and experimental demonstration,’’ IEEE Trans. Antennas Propag., vol. 65, no. 12, pp. 6250–6261, Dec. 2017.

Observing plasma structures at multiple scale sizes in the high-latitude ionosphere with a suite of ground-based instrumentation.

Maguire, S.J.[1], Wood, A.G.[1], Themens, D.R.[1], and McKay, D.[2]

[1] Space Environment and Radio Engineering (SERENE), University of Birmingham

[2] Metsähovi Radio Observatory, Aalto University, Finland

The terrestrial ionosphere is a highly variable medium that affects the propagation of radio waves. Within the ionosphere, large-scale structures, such as polar cap patches, auroral forms, blobs, and polar holes, have been observed. Small-scale irregularities associated with these large-scale structures result from instability processes which can lead to scintillation of trans-ionospheric radio signals, such as those used for Global Navigation Satellite Systems (GNSS). To investigate plasma irregularities and scintillation in the high-latitude ionosphere, the Scintillation and Plasma Density Gradients (SGRAD) and the Scales of Ionospheric Plasma Structuring (SIPS) experiments were conducted using a suite of ground-based instrumentation across January of 2023 and 2024.

SGRAD was conducted using the European Incoherent Scatter (EISCAT) radars. SIPS used a wider variety of instrumentation to observe the high-latitude ionosphere across several scale sizes, and this required an array of ground-based instruments, in conjunction with the Swarm satellites. This allowed for the observation and inference of large-scale (several hundred km), medium-scale (several km), and small-scale (less than 500m) plasma structuring using the EISCAT radars, LOw Frequency ARray (LOFAR), the Kilpisjärvi Atmospheric Imaging Receiver Array (KAIRA), and ground-based GNSS receivers. To assist in the interpretation of the results, the Swarm Ionospheric Scintillation (SWIS) methodology was also used, which utilises data from the Swarm satellites to give a spectrum of irregularities to scale sizes down to 500m (Spogli et al., 2022).

These experiments aimed to observe different large-scale structures under varying geomagnetic conditions and to determine which of these are related to the scintillation of GNSS signals. From the SGRAD results, a polar cap patch was observed exiting the polar cap and becoming a boundary blob. We present the first direct observations of multiple plasma structuring mechanisms acting simultaneously to create a blob. Additionally, the scintillation data was analysed to explore the effects of these structures on GNSS scintillation. The analysis of the scintillation data revealed that it is difficult to determine the exact cause of the scintillation due to the presence of large-scale structures and auroral precipitation. The SIPS experiments ran between 3rd January 2024 and 15th January 2024.

The combination of both ground-based and space-based instruments in this experiment, observing and modelling the ionospheric plasma, gives unprecedented coverage of varying scale sizes which is not possible with individual instrumentation alone. Using this array of observations, the relationship between irregularities of varying scale sizes will be discussed, along with the formation and generation of small-scale irregularities due to instability mechanisms and the subsequent scintillation effects which can occur.

Spogli, L., Iman, R., Alfonsi, L., Cesaroni, C., Jin, Y., Clausen, L., Wood, A., & Miloch, W. J. (2022). *Feasibility of a Swarm Ionospheric Scintillation (SWIS) proxy for L-band scintillation*. AGU Fall Meeting 2022.

Compact Implantable Antenna Design for Leadless Cardiac Pacemaker System

Murray Brown[(1)] and Hongjian Sun[(2)]

[(1)] The University of Durham, Durham, England, UK, (Murray.Brown@durham.ac.uk)
[(2)] The University of Durham, Durham, England, UK, (Hongjian.Sun@durham.ac.uk)

***Abstract*—This paper details an implantable antenna for leadless cardiac pacemaker (LCP) applications operating in the Industrial Scientific Medical (ISM) frequency band (2.4–2.48GHz). Compared to similar literature designs, the antenna uses a shorting pin to achieve an improved simulated 10dB fractional bandwidth of 20%. It implements a spiral-shaped meander pattern in an ultra-compact 3x3x0.5 mm^3 footprint.**

I. Introduction

LCPs attempt to reduce complications and infections caused by conventional wired pacemakers. The limited space inside implantable medical devices (IMDs) necessitates miniaturising implantable antennas.

II. Antenna Design and Simulation Results

A key property of implantable antennas is they must be biocompatible. This antenna would need to be coated in a thin film of ceramic aluminium oxide, as the dielectric used is not biocompatible. The antenna design is presented in fig. 1. The design includes a substrate and superstrate of dielectric

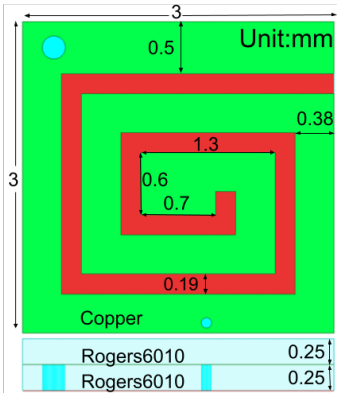

Fig. 1. Suggested antenna structure

material. Rogers6010 was selected due to its high dielectric constant of 10.2. The antenna was modelled and optimised at the centre of a homogeneous heart phantom 60x60x150 mm^3. A conductivity of 2.215 S/m and dielectric permittivity of 54.918 were used to model heart tissue at 2.45 GHz. Fig. 2 shows the S11 of the antenna.

III. Conclusion

This paper introduces a compact, implantable antenna design for LCPs operating at 2.45 GHz. The discussed antenna uses a shorting pin to achieve a fractional bandwidth of

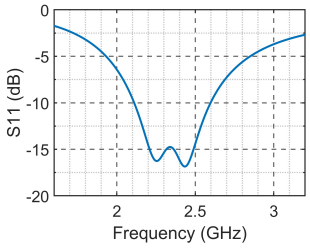

Fig. 2. Simulated reflection coefficient

20% in simulation. This is improved compared to current antennas of similar dimensions at the cost of antenna gain, as summarised in table I. The discussed antenna has an ultra-compact structure at 3x3x0.5 mm^2 [2]. Further research could include implementing ground slots and fabricating the antenna design to observe whether the improved simulated bandwidth carries over to real testing.

ACKNOWLEDGEMENT

This project has received funding from the European Union's Horizon 2020 research and innovation programme under the Marie Skłodowska-Curie grant agreement No 872172 (TESTBED2 project: www.testbed2.org).

References

[1] Muhammad Zada, Izaz Ali Shah, Abdul Basir, and Hyoungsuk Yoo. Ultra-compact implantable antenna with enhanced performance for leadless cardiac pacemaker system. *IEEE Transactions on Antennas and Propagation*, 69(2):1152–1157, 2021.

[2] Yang Feng, Zhaonan Li, Lin Qi, Wanting Shen, and Gaosheng li. A compact and miniaturized implantable antenna for ism band in wireless cardiac pacemaker system. *Scientific Reports*, 12, 01 2022.

TABLE I
Comparison to Existing Literature (simulated 10dB fractional bandwidths were estimated from figures in cited literature)

Ref.	Size (mm^3)	Freq. (GHz)	Simulated fractional 10dB BW (%)	Measured 10dB BW (%)	Peak Gain (dBi)	Phantom Size (mm^3)
[1]	3×4×0.5	2.4	6.5	21.8	-25.9	80×60×120
[2]	3×3×0.5	2.45	7.0	22	-24.9	60×60×150
This Work	3×3×0.5	2.45	20.0	—	-42.7	60×60×150

Ultra-Miniaturized In-Band Full-Duplex Implantable Antenna for Wireless Capsule Endoscopy

Abdullah Alshammari, Amjad Iqbal, Roy B.V.B. Simorangkir, Ismail Ben Mabrouk.
Durham University, Durham, UK. (e-mail: Abdullah.h.alshammari@durham.ac.uk)

Wireless capsule endoscopy (WCE) is a medical diagnostic technique that utilizes a wireless capsule to visualize the gastrointestinal tract (GI). This technology has gained significant attention in recent years due to its non-invasive and painless nature, which provides a better alternative to traditional wired endoscopic procedures [1]-[3]. WCE allows the examination of complex portions of the gastrointestinal tract and overcomes the constraints on patient mobility [4][5]. However, one of the major challenges of WCE is the transmission of the captured images to the external receiver, as the capsule moves through the digestive system. This requires an efficient wireless communication system that can operate at low frequencies mainly because low frequencies can penetrate deeper into the body tissues. This involves a careful balancing of the trade-off between antenna size and transmission range to achieve the desired level of reliability without compromising patient comfort [4]-[6]. This study introduces a novel in-band full-duplex implantable antenna designed for Wireless Capsule Endoscopy (WCE) and operating at the 2.45 GHz Industrial, Scientific, and Medical (ISM) band. The antenna is simulated inside a human body phantom with a depth of 50 mm. The antenna's size is kept ultra-miniaturized ($\pi \times (3)^2 \times 0.254 = 7.17$ mm^3) through the integration of multiple semi-circular slots and shorting pins. The antenna exhibits a nearly omnidirectional radiation pattern at both 2.45 GHz for port 1 and port 2, attaining gains of -44.5 dBi at port 1 and -46.2 dBi at port 2. Achieving higher than 25 dB isolation between the two antenna ports is made possible by using a very thin superstrate and substrate, along with the addition of a middle slot in the ground plane. The antenna is simulated using Ansys High-Frequency Structural Simulator (HFSS) inside a bio-compatible capsule device. In conclusion, the proposed antenna is a promising candidate for implantable medical devices for capsule endoscopy applications, offering and simultaneous transmit and receive capability, high isolation, and compact size.

Index Terms—In Band Full-Duplex, Implantable Antenna, Medical Implants, wireless capsule endoscopy.

REFERENCES

[1] A. Kiourti and K. S. Nikita, "A review of in-body biotelemetry devices: Implantables, ingestibles, and injectables," IEEE Trans. Biomed. Eng., vol. 64, no. 7, pp. 1422–1430, Jul. 2017.
[2] M. Rezapour, C. Amadi, and L. B. Gerson, "Retention associated with video capsule endoscopy: Systematic review and meta-analysis," Gastrointestinal Endoscopy, vol. 85, no. 6, pp. 1157–1168, 2017.
[3] M. Zada and H. Yoo, "A Miniaturized Triple-Band Implantable Antenna System for Bio-Telemetry Applications," in IEEE Transactions on Antennas and Propagation, vol. 66, no. 12, pp. 7378-7382, Dec. 2018.
[4] A. Basir, M. Zada, Y. Cho and H. Yoo, "A Dual-Circular-Polarized Endoscopic Antenna With Wideband Characteristics and Wireless Biotelemetric Link Characterization," in IEEE Transactions on Antennas and Propagation, vol. 68, no. 10, pp. 6953-6963, Oct. 2020.
[5] R. Das and H. Yoo, "A wideband circularly polarized conformal endoscopic antenna system for high-speed data transfer," IEEE Trans. Antennas Propag., vol. 65, no. 6, pp. 2816–2826, Jun. 2017.
[6] L. Wang, T. D. Drysdale, and D. R. S. Cumming, "In situ characterization of two wireless transmission schemes for ingestible capsules," *IEEE Transactions on Biomedical Engineering*, vol. **54**, no. 11, pp. 2020–2027, 2007.

300 GHz Stacked AFSIW LTCC Horn Array Antenna with Integrated Lenses for V2V

Eryk S. Skalinski, Roy B. V. B. Simorangkir, and Ismail B. Mabrouk

***Abstract*—This paper explores the design of a 220-300 GHz horn array in LTCC technology for vehicular communications. An air-filled SIW approach allows compact horn elements with 0.51λ spacing to avoid grating lobes. The integrated Rexolite plano-convex lenses provide additional gain and sidelobe suppression. The 4x6x2.11 mm 1x4 array has a peak gain of 17.5 dBi from 220-340 GHz, a return loss below -10dB, and cross-coupling below -18dB. At 300 GHz, the gain is 15.9 dBi with 30° x 22° HPBWs. Beam steering up to 18° is achieved with only 1.1 dB gain reduction. The design enables practical sub-THz antennas for connected vehicles.**

I. Introduction

In the rapidly advancing realm of wireless communication, 6G holds promising prospects for autonomous vehicles. Developing specialized antennas for sub-THz band vehicular communication is crucial. This work focuses on creating an electronically steerable linear array antenna using LTCC, ensuring protection and mass-manufacturability. Unlike previous methods [1], [2], this approach minimizes grating in the radiation pattern. Simulation results using ANSYS HFSS are detailed in this paper.

II. LTCC Horn Array Antenna

A. Design of antenna

An Air-Filled-Substrate-Integrated Waveguide (AFSIW) H-plane horn, integrated into a multilayer LTCC substrate, enables lower power loss than traditional SIWs for increased power handling [3]. Despite the H-plane horn's ridged radiation pattern, stacking them forms an array with optimal 0.5λ spacing. Metal plates provide isolation, avoiding the need for via fencing. A semicircular plano-convex Rexolite 1422 lens enhances gain, squashing the sectoral horn pattern, and acts as a practical radome. A modified WR-3 feed is driven by LTCC layer thickness, with $\epsilon_r = 6.7$ and $\tan\delta = 0.02$. The antenna array design achieves 0.51λ spacing at 300 GHz with a 100 µm LTCC layer, reducible with a 50 µm variant.

B. Results

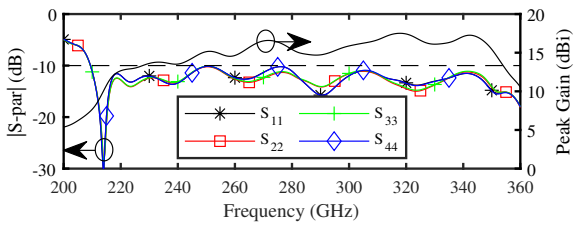

(a)

Fig. 1: Antenna array simulation results: Reflection coefficients and total peak gain

In fig. 1a, return coefficients stay below -10dB across the 220-340 GHz bandwidth, and cross-coupling remains under -18dB (max: -19.4dB). A peak gain of 17.5 dBi is achieved at 318 GHz. At 300 GHz, figs. 1a and 2 show a total gain of 15.9 dBi, with horizontal HPBW of 30° and vertical of 22°. The main lobe shifts from boresight to 18° in the xz plane with only a 1.1 dBi gain reduction, maintaining a side-lobe level below 13.8 dBi at 33°. The xy-plane radiation pattern remains unaffected.

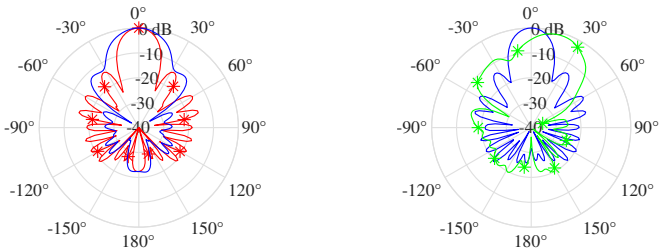

(a) (b)

Fig. 2: Simulated normalized total radiation pattern at 300 GHz: (a) 0 phase difference between each subsequent element normalized in 2 different planes. H/xy-plane or (Red-star), E/xz-plane (Blue), (b) 60 degree phase difference between each subsequent element normalized to non-phased. Standard (Blue), Shifted (Green-star) in E/xz-plane

III. Conclusions

In summary, a protective linear 1x4 H-plane sectoral horn array with lenses, based on AFSIWs in LTCC, was introduced. It offers broad bandwidth, low grating, and effective cross-coupling, making it suitable for V2V. The design is nearly ready for manufacturing and validation through measurements. Integration of a microstrip to waveguide transition is pending, demonstrating the potential for an RFIC integrated within LTCC to serve as an antenna in a package module.

References

[1] S. Rey, T. Merkle, A. Tessmann, and T. Kürner, "A phased array antenna with horn elements for 300 ghz communications," in *2016 International Symposium on Antennas and Propagation (ISAP)*. Ieee, 2016, pp. 122–123.

[2] Z.-Y. Zheng, Z.-J. Shao, and J.-F. Mao, "A 300-ghz step-profiled corrugated horn antenna array," in *2018 IEEE International Symposium on Antennas and Propagation; USNC/URSI National Radio Science Meeting*. Ieee, Jul. 2018.

[3] T. Tajima, H.-J. Song, K. Ajito, M. Yaita, and N. Kukutsu, "300-GHz step-profiled corrugated horn antennas integrated in LTCC," *IEEE Transactions on Antennas and Propagation*, vol. 62, no. 11, pp. 5437–5444, Nov. 2014.

3D Printed Wideband Dual-Polarized Lens Antenna for mm-Wave Communication

Valentina Cicchetti, Queen Mary University of London

Abstract

In the past few years, the popularity of millimeter-wave (mm-wave) frequencies has increased significantly because of the growing need for high-speed wireless communications and the introduction of new applications. The design of antennas for this frequency range should be characterized by high gain to prevent free-space attenuation and support wide bandwidths while maintaining good radiation efficiency and reliable radiation patterns [1]. These requirements lead to structural complexity, and to the miniaturization of antennas, challenging existing manufacturing processes. Three-dimensional (3D) printing technology, also known as additive manufacturing, has gained wide attention as it enables rapid prototyping, low cost and high material utilization while producing high-quality structures. Through this technology, it is possible to realize structure using a layer-by-layer stacking process, allowing for the creation of complex shapes and the achievement of small-scale manufacturing. These advantages could potentially meet the requirements of the antennas at mm-wave frequencies [2]. The purpose of this work is to present a 3D printed wideband dual-polarized lens antenna useful for future mm-wave applications. The proposed antenna consists of a rectangular waveguide WR-10 used as the feeding for the input signal, a rectangular-circular transition that converts the fundamental mode TE10 of the rectangular waveguide to the fundamental mode TE11 of the circular waveguide placed at the end. In addition, a metal cone was designed to distribute the field radiated by the circular guide along the azimuthal plane through a reflection phenomenon [3]. Finally, a dielectric lens, characterized by a toroidal shape and a spherical-axicon section [4], was designed to improve the performance of the radiative structure. The antenna works in the 75-100 GHz frequency range, providing a maximum gain of 9 dBi in the azimuth plane. CST Microwave Studio, implementing a full-wave locally conformal finite integration technique (FIT), was employed to characterize the antenna and to guide its physical realization. A good agreement was found between the numerical results and the experimental measurements performed on an antenna prototype. The structure offers the advantages of robustness, cost-effectiveness, and ease of fabrication in waveguide configurations.

References

[1] R. Xu et al., "A Review of Broadband Low-Cost and High-Gain LowTerahertz Antennas for Wireless Communications Applications," in IEEE Access, vol. 8, pp. 57615-57629, 2020.

[2] Y. Wang, et al. "3D Printed Antennas for 5G Communication: Current Progress and Future Challenges." Chinese Journal of Mechanical Engineering: Additive Manufacturing Frontiers (2023): 100065.

[3] P.K. Verma, R. Kumar and M. Singh, "Design of a shaped omnidirectional circular waveguide antenna," 2009 Applied Electromagnetics Conference (AEMC), Kolkata, India, 2009, pp. 1-3.

[4] R. Cicchetti, V. Cicchetti, A. Faraone, L. Foged and O. Testa, "A Wideband High-Gain Dielectric Horn-Lens Antenna for Wireless Communications and UWB Applications," in IEEE Transactions on Antennas and Propagation, vol. 71, no. 2, pp. 1304-1318, Feb. 2023.

URSI UK Symposium, Teddington, UK, 21 February 2024

Linear Precoding as an Interference Mitigation Technique in a Phased Array Gateway for large LEO Constellations

Francesco Lisi*(1), Carol Marsh(2), Ed Totten(2), and George Goussetis(1)
(1) Heriot-Watt University, Edinburgh, UK, {f.lisi, g.goussetis}@hw.ac.uk
(2) Celestia UK, Edinburgh, UK, {cmarsh,etotten}@celestia-uk.com

Active Electronically Scanned Arrays (AESA) constitute a promising technology for the replacement of reflector antennas as ground stations (GS) for a Low Earth Orbit (LEO) satellite constellation. While only one satellite can be tracked per antenna in the latter systems, the formers allow to simultaneously synthesize multiple beams from the same aperture by applying beamforming, ideally replacing an entire reflector-based antenna farm with a single AESA-based GS. While a teleport with several tens of reflectors could still be less expensive than one with a few AESA, the advancements in microwave monolithic integrated circuits combined with the growth of satellites in LEO constellation suggest that satellite operators will gradually transition to the latter technology[1]. Moreover, AESA guarantee several other benefits, such as graceful degradation, longer time to failure, ease-of-replacement, almost negligible downtime, full hemispherical coverage, and higher pointing accuracy.

The most important feature of AESA systems consists in the possibility of exploiting a variety of beamforming techniques. While analogue beamforming is easier to implement and less expensive, it requires as many parallel beamforming networks as the number of beams to generate. Consequently, digital beamforming is likely to become the adopted technology for LEO constellations in the future decades. In a fully digital beamforming network, each radiating element is connected to an output port that integrates a digital-to-analogue converter, and all the beams' signals are digitally generated. Despite matched filter (MF) precoding provides the highest composite pattern gain, several precoding techniques allow to mitigate the interference generated to adjacent satellites. Two of the most adopted linear precoding techniques are zero forcing (ZF) and minimum mean square error (MMSE) [2]. By slightly sacrificing the main beam gain, they allow to generate composite patterns with nulls located at the other satellites location as shown in Fig. 1. MMSE precoding consists in a trade-off between the MF and ZF ones and guarantees the best performance in terms of SNIR. This work investigates the impact of linear transmit precoding to mitigate the interference in a gateway antenna operating in V band.

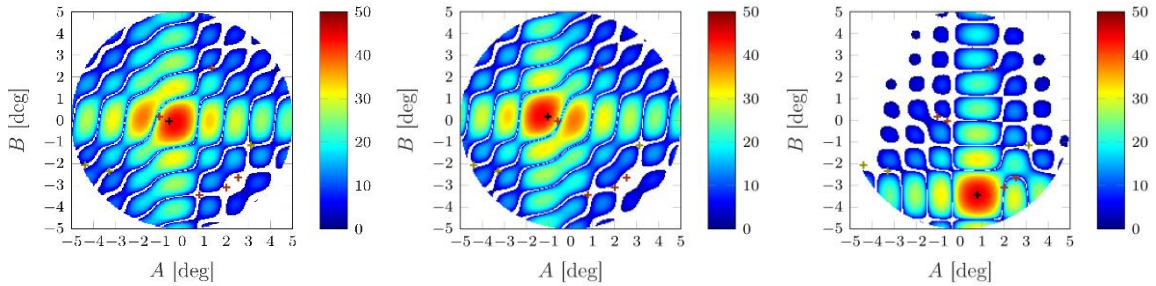

Figure 1. MMSE precoding composite pattern gain (dBi) of three different satellites. The black cross corresponds to the targeted satellite, the red ones to other satellites served by the gateway, and the green ones to non served satellites in the field-of-view.

[1] G. He, X. Gao, L. Sun, and R. Zhang, "A review of multibeam phased array antennas as LEO satellite constellation ground station," *IEEE Access*, vol. 9, pp. 147142–147154, 2021.
[2] P. Angeletti and R. De Gaudenzi, "A Pragmatic Approach to Massive MIMO for Broadband Communication Satellites," *IEEE Access*, vol. 8, pp. 132212–132236, 2020.

Compact Implantable Antenna with Ultra-wide bandwidth for Leadless Pacemaker

Abdulwahab Alghamdi, Roy B. V. B. Simorangkir, and Ismail ben Mabrouk
Durham University, Durham, England, UK (abdulwahab.alghamdi@durham.ac.uk)

***Abstract*—This article introduces a compact antenna designed for leadless pacemakers (LPs), featuring a small size of $8.83\,mm^3$, and a bandwidth of 4330 MHz, addressing detuning issues. Covering frequencies from 0.67 GHz to 5 GHz, the antenna ensures optimal performance in medical frequency bands. The achievement of ultra-wide bandwidth is attributed to integrating a meandered line in the ground plane and a large rectangular slot in the patch. Moreover, the proposed antenna demonstrates high gain values of -31.3 dBi, -25.7 dBi, and -22.7 dBi at 0.915 GHz, 1.4 GHz, and 2.45 GHz, respectively.**

I. Introduction

The demand for compact antennas integrated into LPs for heart telemetry is on the rise. These antennas aim to facilitate the transmission of diverse health-related data, enabling continuous monitoring of patients' cardiac activity during their daily routines [1], [2]. [3]. Infections in conventional pacemakers are a significant concern, affecting approximately one in fourteen patients, with one-fifth of infected patients facing fatal outcomes [4].

The integration of miniaturized implantable antennas into (LPs) plays a pivotal role in enabling wireless data transfer between LPs and external devices [5]. This integration further allows physicians to conduct remote diagnoses and monitor patients [6]. However, miniaturized antennas present unique challenges. Smaller implantable antennas tend to be less effective with lower gains compared to larger counterparts in free space. Achieving impedance matching becomes more challenging as antenna size is reduced, potentially leading to decreased efficiency and signal degradation [7]. Additionally, the issue of detuning arises due to frequency shifts caused by variations in the electrical properties of bodily tissues [8].

II. Antenna Design

The complete geometric model of the proposed implantable antenna, with dimensions of 5.8 mm x 6 mm x 0.254 mm, is illustrated in Fig. 1. In Fig. 1(a), the radiating patch exhibits a rectangular configuration, featuring a significant rectangular cut. Fig. 1(b) illustrates the ground plane in detail, designed with a meandering shape and incorporating an open-ended slot. This design significantly contributes to bandwidth enhancement. The choice of Rogers 3003 material for both the substrate and superstrate is driven by its specific properties, which include a low tangent loss ($\tan\delta$) of 0.0010 and a relatively low dielectric constant (ε_r) of 3.

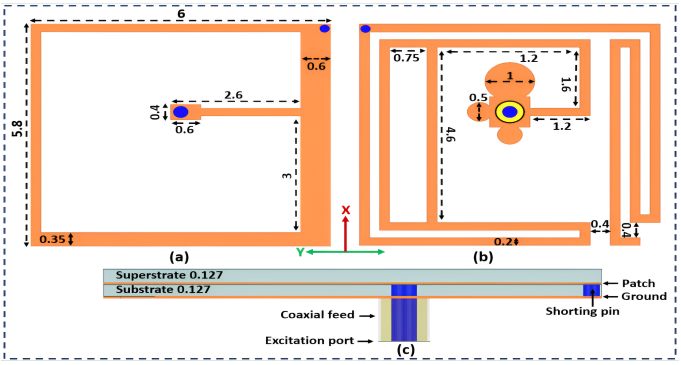

Fig. 1. Geometry of the proposed implantable antenna. (a) Front view, (b) back view, (c) Side view (units: mm).

III. Simulation Setups

The antenna design was implemented using the HFSS (High Frequency Simulation Software). The implantable antenna is positioned within a heart phantom (HP) with dimensions of 120 mm x 80 mm x 60 mm, as illustrated in Fig. 2(a). Its electrical properties for different frequencies (0.915, 1.4, and 2.45 GHz) are adjusted according to Table I. The proposed antenna maintains stable impedance matching in various scenarios, with and without LP, as depicted in Fig. 2(b).

TABLE I
Dielectric properties at various frequencies

Phantom type	Frequency (GHz)	Conductivity (S/m)	Relative permittivity
HP	0.915	1.2378	59.796
	1.4	1.5132	57.538
	2.45	2.2561	54.814

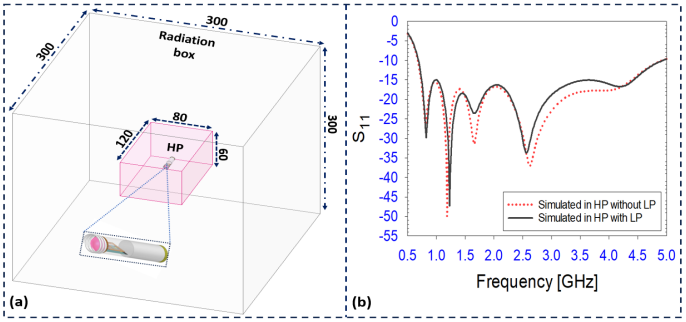

Fig. 2. (a) Antenna implantation in a heart phantom (units: mm), and (b) results in simulated reflection coefficient S_{11}.

REFERENCES

[1] D. G. Della Rocca, C. Gianni, L. Di Biase, A. Natale, and A. Al-Ahmad, "Leadless pacemakers: State of the art and future perspectives," *Cardiac Electrophysiology Clinics*, vol. 10, no. 1, pp. 17–29, 2018.

[2] M. Parvez Mahmud, N. Huda, S. H. Farjana, M. Asadnia, and C. Lang, "Recent advances in nanogenerator-driven self-powered implantable biomedical devices," *Advanced Energy Materials*, vol. 8, no. 2, p. 1701210, 2018.

[3] M. Rav Acha, E. Soifer, and T. Hasin, "Cardiac implantable electronic miniaturized and micro devices," *Micromachines*, vol. 11, no. 10, p. 902, 2020.

[4] S. M. Asif, J. W. Hansen, A. Iftikhar, D. L. Ewert, and B. D. Braaten, "Computation of available rf power inside the body and path loss using in vivo experiments," *IET Microwaves, Antennas & Propagation*, vol. 13, no. 1, pp. 122–126, 2019.

[5] S. M. Asif, A. Iftikhar, B. D. Braaten, D. L. Ewert, and K. Maile, "A wide-band tissue numerical model for deeply implantable antennas for rf-powered leadless pacemakers," *IEEE Access*, vol. 7, pp. 31031–31042, 2019.

[6] A. Joury, T. Bob-Manuel, A. Sanchez, F. Srinithya, A. Sleem, A. Nasir, A. Noor, D. Penfold, R. Bober, D. P. Morin, *et al.*, "Leadless and wireless cardiac devices: The next frontier in remote patient monitoring," *Current Problems in Cardiology*, vol. 46, no. 5, p. 100800, 2021.

[7] M. M. Soliman, M. E. Chowdhury, A. Khandakar, M. T. Islam, Y. Qiblawey, F. Musharavati, and E. Zal Nezhad, "Review on medical implantable antenna technology and imminent research challenges," *Sensors*, vol. 21, no. 9, p. 3163, 2021.

[8] N. Vidal, S. Curto, J. M. Lopez-Villegas, J. Sieiro, and F. M. Ramos, "Detuning study of implantable antennas inside the human body," *Progress In Electromagnetics Research*, vol. 124, pp. 265–283, 2012.

Ultrashort Electromagnetic Pulse System for biological application

Sihao Chen [(1)], Liyang Yu* [(1)], and Wen Dang [(2)]
(1) Hangzhou DianZi University, HangZhou, China, 310018, e-mail: 13754343609@163.com; yuliyang@hdu.edu.cn

This brief introduces a high-voltage ultrashort electric pulse system with a repetition rate with 1 Hz for stimulating cell electroporation tests [1, 2]. This system is designed for stimulating cell electroporation tests [1, 2]. The topology of the given system primarily comprises two parts: high-voltage controlled switch and charging/discharging energy module respectively. An optical-coupler plays a dual-roles, serving as a driver gate to supply the drive signal while providing high isolation [3,4]. A Silicon Carbide (SiC) metal-oxide-semiconductor field-effect transistor (MOSFET) is interconnected with the optical-coupler, collectively forming a voltage-controlled switch. Subsequently, an energy capacitor in series is initially charged up to 1 kV through high-voltage power. The stored energy is then discharged in a controlled manner by the voltage-controlled switch into the cell. As a result, the presented system can provide a stable high-voltage pulse signal with a tunable pulse width ranging from 100 ns to 500 ns.

The schematic diagram of the presented electric pulse generator is depicted as shown in Fig.1. As can be seen, the initial signal, a 3.3 V digital signal generated by the FPGA, triggers the optical-coupler, the ceramic capacitor with a value of 1 uF is connected in parallel to stabilize the operation of a high-gain linear amplifier. The energy capacitor C_e is under direct control of the high-voltage switch, facilitating the charging/discharging process into the cell load.

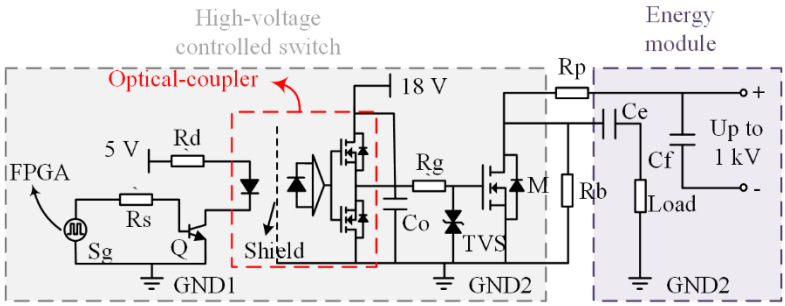

Figure 1. The Schematic Diagram of the Given Electric Pulse System

Reference

[1]. Davies IW, Merla C, Casciati A, et al. "Push–pull configuration of high-power MOSFETs for generation of nanosecond pulses for electropermeabilization of cells," International Journal of Microwave and Wireless Technologies. 2019;11 (7): 645-657. doi:10.1017/S1759078719000576.

[2]. I. W. Davies et al., "Push-Pull Configuration of High Power MOSFETs for Generation of Nanosecond Pulses for Electropermeabilization of Isolated Cancer Stem Cells," 2018 48th European Microwave Conference (EuMC), Madrid, Spain, 2018, pp. 866-869, doi: 10.23919/EuMC.2018.8541734.

[3]. N. Anurag and S. Nath, "Effect of Optocoupler Gate Drivers on SiC MOSFET," 2021 National Power Electronics Conference (NPEC), Bhubaneswar, India, 2021, pp. 01-06, doi: 10.1109/NPEC52100.2021.9672531.

[4]. S. Hwang et al., "GaN-Based 4-MHz Full-Bridge Electrosurgical Generator Using Zero-Voltage Switching Over Wide Load Impedance Range," in IEEE Transactions on Biomedical Circuits and Systems, vol. 17, no. 5, pp. 1125-1134, Oct. 2023, doi: 10.1109/TBCAS.2023.3310880.

Near-Field Velocity Sensing

Zhaolin Wang*, Xidong Mu*, Yuanwei Liu*

*Queen Mary University of London, London E1 4NS, United Kingdom.

Abstract: The near-field and far-field are the two inherent electromagnetic field regions associated with antenna arrays. Due to the small aperture of the antenna array and the low carrier frequency, current wireless networks operate mainly in the far-field region. However, with the advent of Extremely Large Aperture Arrays (ELAA) and the use of higher frequency bands such as millimeter-wave and terahertz bands, recent studies have shown that the near-field region may extend to tens or even hundreds of meters. There are two key differences in near-field systems when compared to far-field systems: 1) the signal phase changes have to be modeled accurately using the spherical-wave model and 2) the user/target has different velocity projections for different antennas, resulting in non-uniform Doppler frequencies. Generally, the velocity of the target is estimated based on the Doppler frequency encapsulated in echo signals reflected by the target. The far-field systems exhibit uniform Doppler frequencies across all antennas introduced by the radial velocity, i.e., the velocity projection aligned with the direction between the BS and the target. In this case, since only partial velocity information is available, determining the target's motion status necessitates prior knowledge of the target's motion model or collaboration among multiple sensing nodes. However, the near-field effect revolutionizes velocity sensing by introducing non-uniform Doppler frequencies that capture not only radial but also transverse velocities. This unique characteristic enables the estimation of the target's motion status, encompassing both the amplitude and direction of the velocity, using a single BS, without necessitating prior knowledge of the target's motion model. With full velocity information, predicting the target's subsequent location becomes simpler and more efficient. This heightened sensing capability can also greatly simplify various communication tasks like beam tracking, channel estimation, and cell handover that are sensitive to users' location.

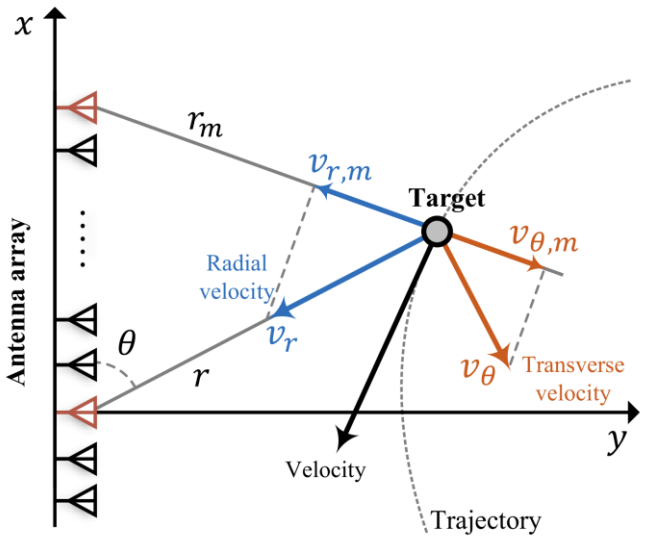

Fig. 1: Illustration of the near-field velocity sensing.

A Compact Conformal Capsule Antenna For MIMO Operation

Liu Chang[(1)], Amjad Iqbal[(1)], Abdul Basir[(2)], Roy B. V. B. Simorangkir[(1)], and Ismail Ben Mabrouk[(1)]

[(1)] Department of Engineering, Durham University, Lower Mount Joy, South Road, Durham, DH1 3LE
[(2)] Tampere University, Kalevantie 4, 33100 Tampere, Finland

***Abstract*—This paper presents a compact, mirror-symmetrical, and meander-structured MIMO conformal antenna for wireless capsule endoscopy. Measuring 30.5 mm x 5.65 mm x 0.04 mm (6.893 mm³ volume), the antenna operates between 0.83 GHz and 1.06 GHz, with a peak resonance at 915 MHz, a bandwidth of 230 MHz (25.14% fractional bandwidth), and 21 dB isolation. Simulations show a -46 dBi gain at 133 mm implantation depth in the human body. The antenna's performance is stable across various tissue dielectric constants, ensuring sufficient Link Margin and safe SAR levels, making it suitable for high-data-rate bio-telemetry.**

I. Introduction

Nowadays, as the next generation of communication technology developed, researchers increasingly prioritize the development of remote health diagnosis and monitoring equipment. Among these, the investigation of ingestion and implantable medical devices hold particular significance. These devices play a crucial role in the medical field, including applications such as pacemaker [1], intracranial pressure monitor [2], blood glucose monitor [3], and wireless capsule endoscopy (WCE) [4]. Among them, WCE is generally used to examine the gastrointestinal tract, particularly the small intestine, which is a blind zone for traditional endoscopy. WCE can help diagnose by transmitting real-time video or high-resolution pictures, overcoming imposed by traditional endoscope size. Generally, a WCE principally comprises a power source, a camera or multiple sensor, and transmission antenna. This antenna plays a pivotal role in sending data, gathered by the sensor or imaging device, to an external receiver. To guarantee efficient and uninterrupted data transfer, it is important for the WCE's antenna to possess robust data transmission capabilities. Recent studies have introduced various capsule antenna in [5], [6]. In [5], a proposal for ultra-wideband antenna is presented, featuring a step-shape and combined with an irregular rectangular loop. This design achieves a bandwidth range from 2.15GHz to 14.75GHz and measures 21.7 mm $\times$ 14.8 mm $\times$ 0.8 = 256.928 mm^3. Besides, in Paper [6], a meandering mode design is employed to encompass both the Industrial, Scientific, and Medical (ISM) band (433 MHz-434 MHz) and the Wireless Medical Telemetry Services (WMTS) band (1.312 GHz-1.644 GHz). The design achieves bandwidths of 442 MHz (210–652 MHz) and 332 MHz (1.312–1.644 GHz) for the ISM and WMTS bands, respectively. However, it is noted that the aforementioned designs are based on single-input single-output (SISO) configurations. In contrast, multi-input multi-output (MIMO) structured antennas typically offer greater channel capacity. Consequently, to facilitate high-performance communication, a compact dual-element antenna operating at 915MHz, with dimensions of 6.893mm^3, is proposed.

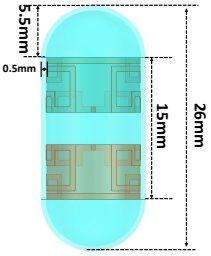

Fig. 1. Loop antenna structure and capsule dimension

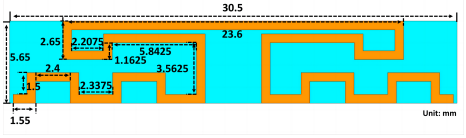

Fig. 2. Plane antenna structure with parameters

This paper introduces a compact, conformal capsule antenna, specifically developed for wireless capsule endoscopes. Utilizing a MIMO configuration, the antenna attains compactness by incorporating mirror symmetry and a meander structure, measuring 6.893 mm^3 in dimensions. Both modules of the antenna operate at 915 MHz, featuring a bandwidth of 230 MHz and a fractional bandwidth (FWB) of 25.14% with isolation 21dB. The stability and safety of the antenna have been thoroughly verified.

References

[1] K. Y. Yazdandoost and R. Miura, "Miniaturized uwb implantable antenna for brain-machine-interface," in *2015 9th European Conference on Antennas and Propagation (EuCAP)*. IEEE, 2015, pp. 1–5.

[2] D. Popovic, M. Khoo, and S. Lee, "Noninvasive monitoring of intracranial pressure," *Recent Patents on Biomedical Engineering (Discontinued)*, vol. 2, no. 3, pp. 165–179, 2009.

[3] J. S. Krouwer and G. S. Cembrowski, "A review of standards and statistics used to describe blood glucose monitor performance," *Journal of Diabetes Science and Technology*, vol. 4, no. 1, pp. 75–83, 2010.

[4] I. M. Mehedi, K. P. Rao, F. M. Alotaibi, and H. M. Alkanfery, "Intelligent wireless capsule endoscopy for the diagnosis of gastrointestinal diseases," *Diagnostics*, vol. 13, no. 8, p. 1445, 2023.

[5] R. Li and Y. Guo, "A conformal uwb dual-polarized antenna for wireless capsule endoscope systems," *IEEE Antennas and Wireless Propagation Letters*, vol. 20, no. 4, pp. 483–487, 2021.

[6] M. J. Christoe, N. Phaoseree, J. Han, A. Michael, S. Atakaramians, and K. Kalantar-Zadeh, "Meandering pattern 433 mhz antennas for ingestible capsules," *IEEE Access*, vol. 9, pp. 91 874–91 882, 2021.

Multiple-Element Smartphone Antenna Design with Broadband Resonators for 5G Cellular Communications in Sub 6 GHz Spectra

H. J. Basherlou [(1)], N. O. Parchin [(1)], L. Manjakkal [(1)], C. H. See [(1)], and R. A. Abd-Alhameed [(2)]

(1) SCEBE, Edinburgh Napier University, Edinburgh, EH10 5DT, UK
(2) Faculty of Engineering and Informatics, University of Bradford, Bradford BD7 1DP, UK

This study proposes a novel MIMO antenna design comprising four pairs of compact dual-polarized antennas strategically positioned at the four corners of the smartphone's mainboard. The antenna structure is realized on an inexpensive FR-4 substrate. Each antenna element incorporates a trapezoid-shaped slot resonator complemented by an L-shaped stub. To enhance the isolation between adjacent slot antennas, an arrow-shaped strip serves as a decoupling structure. The compact antenna elements efficiently operate within the frequency range of 3.35-6 GHz, exhibiting dual-polarization functionality and providing full radiation coverage, ensuring comprehensive connectivity. The properties and performance of the CPW-fed slot antenna element, as well as the entire MIMO smartphone design, are meticulously evaluated using CST software. Through rigorous simulations, the MIMO antenna system's capabilities and efficacy are investigated, and acceptable results have been discovered.

Figure 1(a) depicts the structural configuration of this multi-feed antenna system. The overall size of the antenna is 75×150 mm², and it features 8×8 closely spaced trapezoidal slot resonators with L-shaped stubs and CPW feedings. The S-parameters of the designed antenna array shown in Fig. 2(b) and (c) indicate that the antenna elements have similar performance and provide high matching offering better than -15 dB reflection coefficients (S_{nn}) with mutual coupling (S_{m1}) less than -13 dB at the desired broad operation frequency of band of 3.2-6 GHz. Figure 2 (a) displays a photograph of the prototype sample. The antenna is implemented on a single side of a low-cost FR4 substrate and features an 8×8 MIMO configuration. Figure 2 (b) illustrates the feeding method used for the antenna pair. The measured and simulated results of the S-parameters for two closely spaced elements under test are presented in Figure 2(b) for comparison. As observed, the antenna design achieves a quite good impedance bandwidth (S_{11} < -10 dB) that spans from 3.2 GHz to over 6 GHz, making it suitable for a wide range of frequency applications. Moreover, the mutual couplings (S_{21}) between the adjacent elements are measured to be less than -14 dB at the desired band.

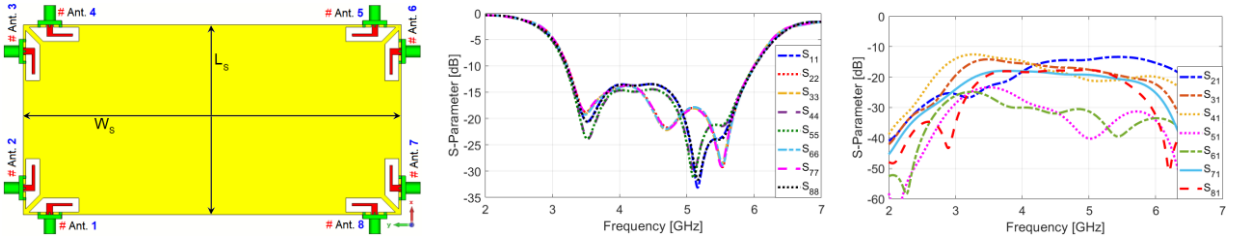

(a) (b) (c)

Figure 1. Proposed MIMO antenna and its simulated (a) S_{nn} and (b) S_{m1}.

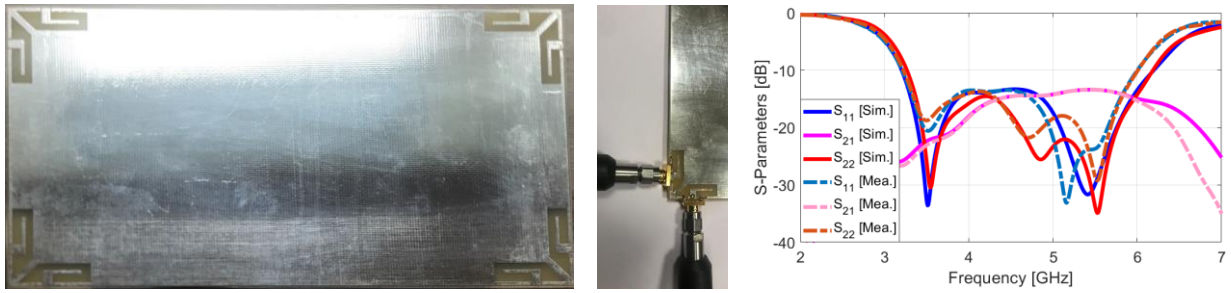

(a) (b) (c)

Figure 2. (a) Fabricated prototype, (b) feeding mechanism, and (b) measured/simulated S_{11}/S_{21}.

A Multiple-stage Uniform Transmission Line Matching Technique for Triple-Band RF-to-DC Rectifier with Harmonic Suppression for Wireless Power Transfer Applications.

M. Odiamenhi, C.H. See, N. Ojaroudi Parchin, H.Yu, and K.Goh

School of Computing, Engineering, the Built Environment, Edinburgh Napier University, 10 Colinton Road, Edinburgh, EH10 5DT, UK
(m.odiamenhi@napier.ac.uk, c.see@napier.ac.uk)

Conventional RF-to-DC single band rectifier has poor power conversion efficiency (PCE) due to only able to harvest one environment's ambient radio frequency source [1]. This issue can be addressed by carefully integrating a nonlinear diode into the rectifier, which is crucial in determining both PCE and bandwidth. Despite this, achieving maximum PCE is hampered by the predominance of diode harmonic loss over network insertion loss [2], [3], limiting the rectifier's output power. To overcome this constraint, it's essential to simultaneously harvest RF energy from multiple sources and effectively terminate harmonics to maximize output power.

The triple-band rectifier proposed in this paper makes use of a harmonic suppression network (HSN) made up of five microstrip transmission lines (TLINs) and a uniform transmission matching approach as shown in Figure 1(a). The HSN effectively suppresses the triple-band signal's second harmonic, resulting in infinite impedance, according to theoretical study based on closed-form equations [1].

The design started with a single-band rectifier and was expanded to dual- and triple-band versions by adding appropriate transmission lines and shorted stubs. To convert multiple RF signals into direct current simultaneously, a harmonic suppression network was introduced. The suggested rectifier achieves PCE of 75.5%, 72%, and 67.1%, respectively, and operates in the widely used frequency bands of 1.8, 2.45, and 5.8 GHz (see Figure 1(b)).

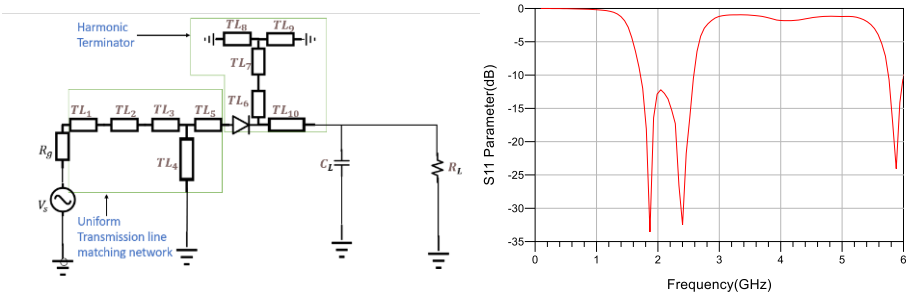

Figure 1: (a) Proposed circuit triple band rectifier with harmonic suppression and (b) Simulated S11 results

References

[1] D. Surender, T. Khan, F. A. Talukdar, and Y. M. M. Antar, "Rectenna Design and Development Strategies for Wireless Applications: A review," *IEEE Antennas and Propagation Magazine*, vol. 64, no. 5. 2022. doi: 10.1109/MAP.2021.3099722.

[2] J. Guo, H. Zhang, and X. Zhu, "Theoretical analysis of RF-DC conversion efficiency for class-F rectifiers," *IEEE Trans Microw Theory Tech*, vol. 62, no. 4, 2014, doi: 10.1109/TMTT.2014.2298368.

[3] D.-A. Nguyen and C. Seo, "A Compact and High-Efficiency Design of 0.915/2.45 GHz Dual-Band Shunt-Diode Rectifier for Wireless Power Transfer," *IEEE Microwave and Wireless Components Letters*, 2022, doi: 10.1109/lmwc.2022.3158337.

URSI UK Symposium 2024

Challenges in Camera Integrated Antenna Design for WCE

Muhammad Qamar[(1)],Kamil Yavuz Kapusuz [(2)], Mohamed A. Thaha*[(1)], and Akram Alomainy**[(1)]
(1) Queen Mary University of London: School of Electronic Engineering and Computer Science, London, UK
(2) Department of Information Technology, IDLab/EM Group, Ghent University/imec, Ghent, Belgium

Wireless capsule endoscopy (WCE) represents a groundbreaking advance in numerous potential imaging/diagnostics applications and an increasing role in digestive pathological examination, providing a non-invasive method to visualize the gastrointestinal (GI) tract. Recently, wireless endoscopy has been enabled by the realization of the swallowable low-power capsule, which includes cost-effective miniaturized integrated circuits, batteries, light-emitted diodes (LEDs), cameras, and antennas. In particular, several limitations, such as stable and robust performance, high data rate, extensive camera viewing angle, and reliable communication link make camera-integrated antenna design for WCE applications very challenging.

Firstly, the designated space for antenna integration without blocking the viewing of the cameras is confined to the pill shaped capsule surface or the area between the camera and the capsule shell [see Fig. 1]. Secondly, the capsule's size and the camera's shape impose limitations on the inclusion of an additional matching network inside the 11×26 mm^2 capsule. In particular, proper antenna feeding might be necessary at the top of the camera body, necessitating meticulous consideration to ensure it does not impact the functionality of the camera lens. Thirdly, the demand for a substantial camera viewing angle requires the deployment of LEDs and a transparent air dome between the optical dome and the camera. Finally, as the capsule traverses through the heterogeneous gastrointestinal environment, it may encounter frequency-detuning effects, necessitating robust antenna performance. This aspect adds a layer of complexity to the antenna design, making it a particularly challenging task.

This contribution describes a novel compact topology to realize camera integration in antenna systems for WCE applications. Specifically, we showcased a planar antenna topology based on offset-fed meandered dipole antenna fabricated by conventional cost-effective printed circuit board (PCB) technology, which can be part of a new generation of cost-effective high-performance systems. The designed antenna was optimized for operation in the [401-406] MHz range in the medical device radio communications service (MedRadio) band.

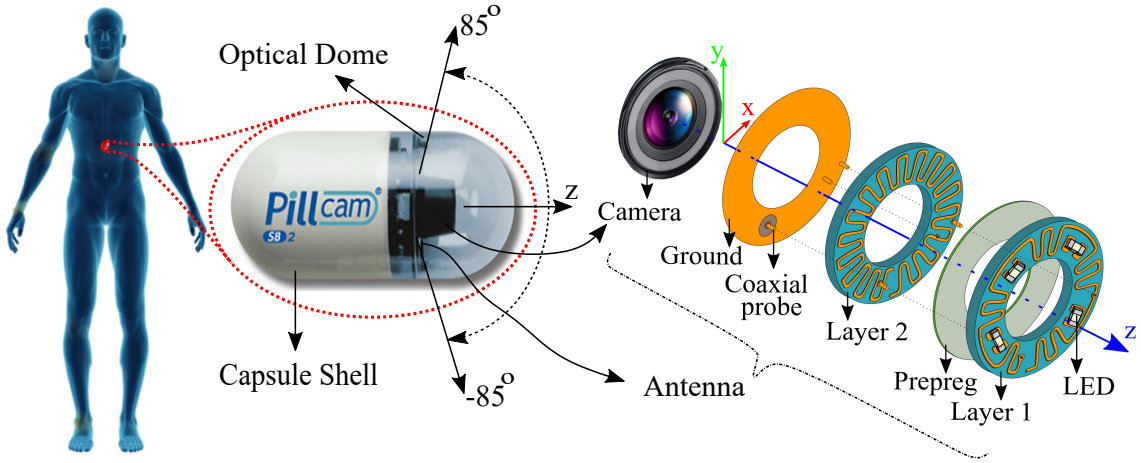

Figure 1. GI tract that the biotelemetric capsule would be able to map and the visible components found within an imaging capsule system with dimensions 11×26 mm^2.

URSI UK Symposium 2024, UK, 21 February 2024

A Ray Tracing Channel Modelling Study for Indoor Sub-THz Propagation between 500 GHz and 750 GHz

Qi Li * (1), (2), Ben Chen (3), Ke Guan (3), Lawrence Carslake (2), Yuan Yao (1), and Tian Hong Loh (2)
(1) Beijing University of Posts and Telecommunications, Beijing, China
(2) National Physical Laboratory, Teddington, United Kingdom
(3) Beijing Jiaotong University, Beijing, China

Abstract

This study focuses on the modelling and simulation of indoor channel scenarios within the 500 GHz-750 GHz sub-terahertz (sub-THz) frequency band, with the aim of enhancing our understanding of channel characteristics at these frequencies. The accuracy of the simulation platform was validated by comparing its results with measured data, thus confirming its reliability. Horn antennas and omnidirectional antennas were utilized during simulations to investigate channel behavior in both obstructed and unobstructed environments. By varying the distance between transmitting (Tx) and receiving (Rx) antennas, channel characteristics within the 500 GHz-750 GHz frequency band were systematically investigated. The figure below shows a comparison using an omnidirectional and a horn antenna in an obstructed scenario.

Our primary contribution lies in the initial exploration of scenario modeling and simulation for indoor channels in the sub-THz frequency band, thereby addressing a critical research gap. This research serves as an indispensable reference for future design and optimization of indoor communication systems. The experimental results provide comprehensive insights into channel characteristics under varying antenna types and environmental conditions, offering valuable data support. Consequently, this work establishes a robust foundation for further research and applications, significantly contributing to the understanding of propagation characteristics for indoor channels within the 500 GHz-750 GHz frequency band.

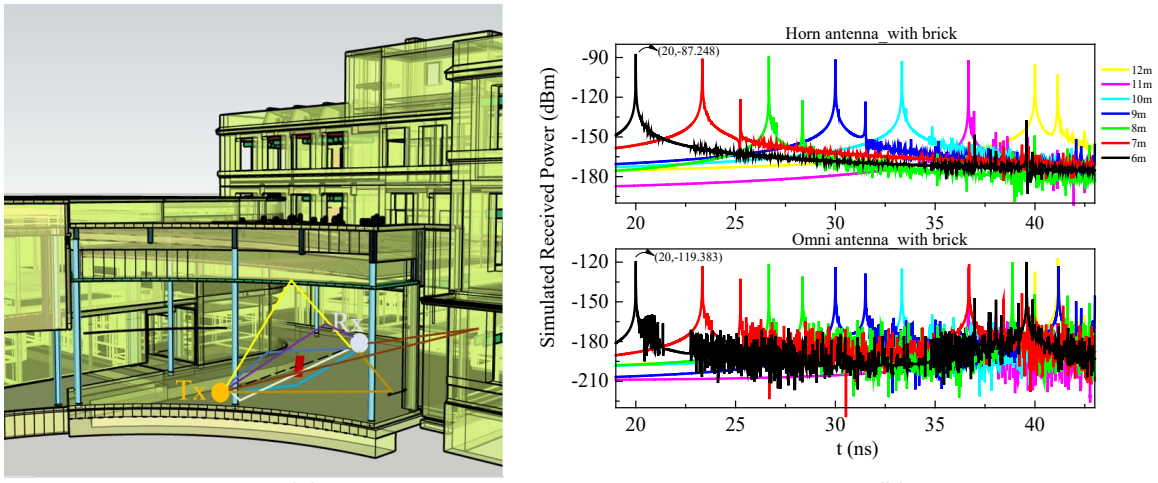

(a) *(b)*

Ray-tracing simulated 3D path-with brick-Omni antenna and Ray-tracing simulated results

Keywords: Indoor, Sub-terahertz, channel characterizations.

Acknowledgements
The work was supported in part by the 2021–2025 National Measurement System Program of the U.K. Government's Department for Science, Innovation and Technology (DSIT), under Science Theme Reference EMT24 of that Program and in part by the project (21NRM03 MEWS), which has received funding from the European Partnership on Metrology, co-financed from the European Union's Horizon Europe Research and Innovation Programme and by the Participating States. Funded by the European Union. Views and opinions expressed are however those of the author(s) only and do not necessarily reflect those of the European Union or EURAMET. Neither the European Union nor the granting authority can be held responsible for them.

Optimising Optical Transparency and RF Performance in Meshed 5G Vehicular Antennas

William J. Bourne, Roy B. V. B. Simorangkir, and Ismail Ben Mabrouk
Department of Engineering, Durham University, DH1 3LE, UK

***Abstract*—With 5G networks enabling new vehicular connectivity services, there is a need for effective antennas to be integrated into automotive glass. As a result, better optically transparent (OT) conductive films are required. This paper analyses micro-scale metal meshes as a promising OT conductor technology. Theoretical analysis suggests that sheet resistance and optical transparency can be tuned using the geometry of the conductive mesh and simulation is conducted. The findings provide design guidelines to optimise the optical and radio frequency performance of metal mesh in vehicle windows.**

I. Introduction

The advent of 5G networks can enhance road safety, reduce energy consumption, and lower congestion [1] This requires that the number and size of antennas increase in diverse user equipment. In vehicle design, mounting antennas in the windows has been suggested [2]. However, antennas can only be placed on windshields if their overall optical transparency (OT) remains greater than 70%. Gains have been made in reducing sheet resistance by using metallic structures. In [3], a silver micro-mesh is fabricated with $R_s = 0.054$ Ω/sq and $T_x = 81.3\%$. These are generally recognised as having: optical properties, electrical properties, mechanical stability and cost that are better than current alternatives. Recently, additive manufacturing methods with lower wastage and costs are being considered for micro-scale metal mesh fabrication. Screen and gravure jet printing enable the mass-production of this OT conductor, with significantly better characteristics than TCOs. However, printed metal conductivity is typically worse than in the bulk material [4]. Because of this, it is important to improve the conductivity of printed metallic meshes. Conductivity improvements have been made by altering the mesh metallic layer at the nano-scale [4], but the electro-optical characteristics also depend significantly on the mesh structure itself. This work investigates how changing the mesh geometry affects the trade-off between the optical and electrical performance of micro-scale metal mesh in the 2 – 10 GHz band.

II. Methodology and Preliminary Results

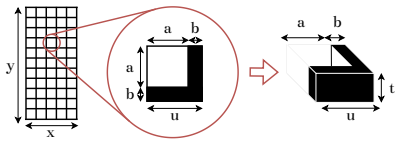

Fig. 1. Layout of a metallic square mesh. The unit cell is shown enlarged.

An example metallic mesh structure is shown in fig. 1. From the unit-cell, it is clear that the DC sheet resistance of the mesh decreases at larger values of b. However, for AC, the current density falls off exponentially below the skin depth (δ) in a good conductor. It follows that increasing the $a : b$ ratio (and so the OT) within each unit cell will have a negligible impact on the mesh AC sheet resistance while $b >> 2\delta$. Simulation was used to investigate the effect of mesh geometry on the impedance of a microstrip transmission line. A silver mesh transmission line was modelled on a glass dielectric. The mesh unit-cell length scale was selected as $u = 589$ μm. The system response in the $2 - 10$ GHz region was measured as the $a : b$ ratio within fixed unit cells was changed. This region was selected to include 5G FR1. While the transmission line remains well-matched throughout the parameter sweep, fig. 2 shows the frequency response of the forward transmission through the line for different widths of b. This is compared with a solid silver microstrip of identical dimensions (the control). At 2 GHz, there is good transmission through all the strips except as b approaches 2δ. As the skin effect becomes stronger at higher frequencies, the mesh conductivity decreases and reduces the forward transmission. It is notable that the meshes generally outperform the bulk material in this region i.e. the S_{21} is less attenuated. The forward transmission is also shown not to improve where $b > 20$ μm.

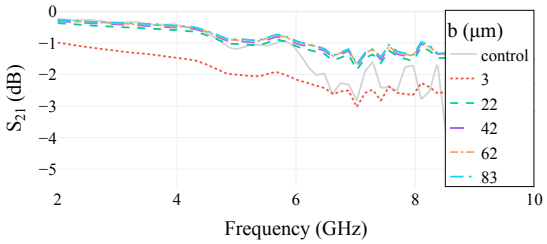

Fig. 2. Forward transmission – frequency relationship.

References

[1] C. R. Storck and F. Duarte-Figueiredo, "A Survey of 5G Technology Evolution, Standards, and Infrastructure Associated With Vehicle-to-Everything Communications by Internet of Vehicles," *IEEE Access*, vol. 8, 2020. 1

[2] A. M. H. Nasr and K. Sarabandi, "A Low-Cost Millimeter-Wave 5G V2X Multi-Beam Dual-Polarized Windshield Antenna," *IEEE Open Journal of Antennas and Propagation*, vol. 3, 2022. 1

[3] J. Hautcoeur, F. Colombel, M. Himdi, X. Castel, and E. M. Cruz, "Large and Optically Transparent Multilayer for Broadband H-Shaped Slot Antenna," *IEEE Antennas and Wireless Propagation Letters*, vol. 12, 2013. 1

[4] W. Li, Z. Akhter, M. Vaseem, and A. Shamim, "Optically Transparent and Flexible Radio Frequency Electronics through Printing Technologies," *Advanced Materials Technologies*, vol. 7, 2022. 1